SCIENCE OF LIGHT

VOLUME 10 NUMBER 2

September
1961

Published by the

Institute for Optical Research

Tokyo University of Education

in collaboration with

The Spectroscopical Society of Japan

SCIENCE OF LIGHT

Science of Light contains reports of the Institute for Optical Research and contribution from other science bodies about similar subjects

All communications should be addressed to the director or to the librarian of the Institute.

The Institute for Optical Research

Tokyo University of Education

400, Hyakunin-tyo-4, Shinzyuku-ku, Tokyo, Japan

Printed by
Kabushiki Kaisha Kokusai Insatsu,
Tokyo

Temperature Dependence of Quadrupole Coupling Constant and Asymmetry Parameter of Para-Diiodobenzene under Constant Pressure

Akira SHIMAUCHI

Institute for Optical Research, Tokyo University of Education
Sinzyuku-ku, Tokyo

(Received March 20, 1961)

Abstract

Quadrupole resonance frequencies of I^{127} in *p*-diiodobenzene are precisely determined by simultaneous measurement between 297.6°K and 77°K. The temperature variations of quadrupole coupling constant, eQq, and asymmetry parameter, η, are investigated in detail under constant pressure.

In order to explain the obtained result, intermolecular torsional oscillations and intramolecular vibrations of fairly low frequencies must be acquainted with, hence Raman spectroscopy and far-infrared spectroscopy of *p*-diiodobenzene are also carried out.

As a result of investigation of Raman lines, frequencies of torsional oscillation are determined as follows: 23, 27 and 116 cm^{-1} at 26.5°C change to 26, 30 and 134 cm^{-1} at 77°K respectively. As for intramolecular low frequency vibration, Raman active C-I bending vibrations seem to correspond to 250 and 286 cm^{-1}, and infra-red active C-I bending frequencies to 143.0 and 145.7 cm^{-1}. With the use of all these frequencies, eQq is evaluated on the assumption that the influence of volume change can be represented by the shift of intermolecular torsional frequencies. Values of eQq thus obtained almost agree with the experiment. Temperature dependence of η can not be fully explained merely by the influence of the above-mentioned frequencies; it seems necessary to take into account the ring vibrations, B_{1u}, B_{2g} and A_g, frequencies of which are taken as 90, 111 and 158 cm^{-1} respectively.

The appearance of low frequency Raman line, 15 cm^{-1}, which is originally of Raman inactive translational mode, has to be ascribed to invalidation of selection rule, otherwise the temperature variations of eQq and η can not be reasonably explained. This reasoning seems also available for *p*-dichlorobenzene.

1. Introduction

The nuclear quadrupole coupling constant generally decreases as the temperature is raised. This fact was studied first by Dehmelt and Krüger[1] on halogen nuclei

1) H. G. Dehmelt and H. Krüger: Z. Physik **129** (1951) 401.

in dichloroethylene and methylbromide, and was explained as an influence of molecular vibrations in crystals. Soon later Bayer[2] proposed a theory dealing with one torsional oscillation, and applied his theory to trans-dichloroethylene. This theory was generalized by Kushida[3] and Wang[4] to explain the main features of this temperature dependent effect. However, as Dautreppe *et al.*[5] indicated, even this revised theory could not sufficiently explain the experimental results. Thereupon Dreyfus *et al.*[6] suggested that temperature dependence of Raman frequencies should be taken into account in such a case of *p*-dichlorobenzene or *p*-dibromobenzene. Kushida *et al.*[7] found that quadrupole resonance frequency depends not only on temperature but also on pressure, and suggested that the theories so far obtained could explain the data that would be obtained if observed under constant volume. Since, up to that time, measurements on temperature dependence of resonance frequency had been made only under constant pressure, it should be noted that several effects due to the change of volume on quadrupole coupling constant, asymmetry parameter and molecular vibrations are involved in the data. Brown[8] has re-investigated quadrupole resonance frequencies under constant pressure and estimated a kind of temperature coefficient under constant volume on the assumption that (i) the quadrupole coupling constant is independent of volume, and (ii) the lattice frequencies vary linearly with temperature.

All these investigations were concerned with chlorine or bromine of nuclear spin 3/2, asymmetry parameter of which can not be determined except by observing Zeeman pattern of a single crystal, and the value obtained by this method can not be precise enough to obtain temperature dependent effect. Since the nucleus of iodine has nuclear spin 5/2, its asymmetry parameter and quadrupole coupling constant can be determined precisely by the use of polycrystalline sample of iodine compound.

In this work, *p*-diiodobenzene, which forms molecular crystals, has been selected to observe temperature dependent effect of quadrupole coupling constant and asymmetry parameter of iodine nucleus. It can be assumed that the change in volume of this sample depends mainly on the variation of intermolecular distances, and not on the change of dimention in a molecule. Therefore, quadrupole coupling constant and asymmetry parameter should be independent of volume, but the frequency of

2) H. Bayer: Z. Physik **130** (1951) 227.
3) T. Kushida: J. Sci. Hiroshima Univ. **A19** (1955) 327.
4) T.C. Wang: Phys. Rev. **99** (1955) 566.
5) D. Dautreppe, B. Dreyfus and M. Soutif: Compt. rend. **238** (1954) 2309.
6) B. Dreyfus and D. Dautreppe: Compt. rend. **239** (1954) 1618.
7) T. Kushida, G.B. Benedek and N. Bloembergen: Phys. Rev. **104** (1956) 1364.
8) R.T.C. Brown: J. Chem. Phys. **32** (1960) 116.

torsional oscillation of molecule of the whole should depend on volume, for this frequency can be affected by the field of crystal. On this basis the obtained results are explained by the use of a theoretical formula derived under constant volume. In the formula the influence of volume change is involved only in the terms relating with the frequencies of torsional oscillations.

Since the temperature dependence of torsional oscillations of *p*-diiodobenzene has not yet been studied, Raman spectra of this sample at room and liquid nitrogen temperatures are observed. Intramolecular vibrations of this sample, frequencies of which are lowered by heavy iodine atoms, are also observed in Raman and far-infrared spectra.

In the formula expressing the temperature dependence of asymmetry parameter, there is a term dependent only on the frequencies of torsional oscillations and intramolecular vibrations. The magnitude of this term is of the order of experimental error when asymmetry parameter is determined by Zeeman pattern. In this work, the temperature dependence of this term is investigated for the first time, because asymmetry parameter can now be worked out precisely by the use of *p*-diiodobenzene.

2. Theory

The nucleus of spin 5/2, similar to that of I^{127}, has two frequencies of pure quadrupole resonance. If the molecules are in stationary state, these two frequencies, ν_{01} and ν_{02}, are expressed by the following formulae,[4)9)]

$$\begin{aligned}\nu_{01}&=\frac{3}{20}eQq_0\left(1+\frac{59}{54}\eta_0^2-\frac{11093}{17496}\eta_0^4\right),\\ \nu_{02}&=\frac{3}{10}eQq_0\left(1-\frac{11}{54}\eta_0^2+\frac{2837}{17496}\eta_0^4\right).\end{aligned}\tag{1}$$

Here eQq_0 is called a quadrupole coupling constant of stationary molecule, q_0 representing q_{0zz}. η_0 is an asymmetry parameter for the field gradient and is given as

$$\eta_0=\frac{q_{0xx}-q_{0yy}}{q_{0zz}}.\tag{2}$$

For $\eta_0>0$, the following relation (3) must hold.

$$|q_{0xx}|<|q_{0yy}|<|q_{0zz}|.\tag{3}$$

Since the iodine of *p*-diiodobenzene is in the state of "*p*-electron defect" and is attached to a benzene ring, the relation (3) can be satisfied if the principal axis

9) R. Bersohn: J. Chem. Phys. **20** (1952) 1505.

system for field gradient is used, namely, Z_I and X_I axes refer respectively to I–I direction and perpendicular to the plane of the benzene ring.[10] If the molecules are assumed to be in torsional oscillations around these three principal axes, such oscillations give exactly the same effect on the quadrupole resonance frequencies of I^{127} nucleus as the torsional motions around X, Y and Z directions shown in Fig. 1. For

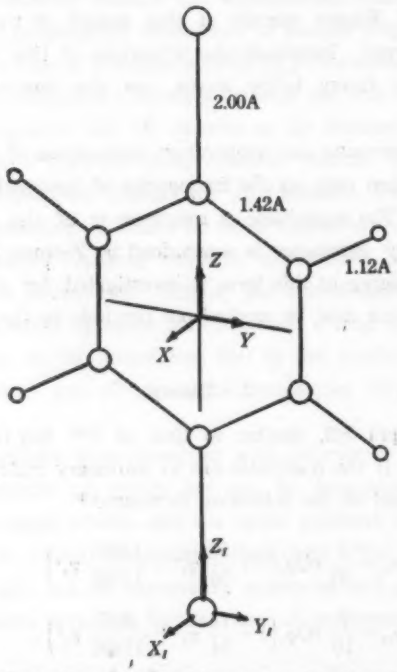

Fig. 1. Dimensions of *p*-diiodobenzene molecule and three principal axes for field gradient of iodine nucleus, and three axes around which torsional oscillation of the whole is considered.

small rotations θ_X, θ_Y and θ_Z about three axes X, Y and Z fixed in the molecule, if only linear and square terms of θ_i ($i=X, Y, Z$) are retained in the expression for the relation between the components of field gradient tensors of space-fixed and molecule-fixed coordinates, the instantaneous field gradient tensor of the oscillating molecule is time-dependent and non-diagonal. But since the observed quadrupole frequencies

10) T. P. Das and E. L. Hahn: "Nuclear Quadrupole Resonance Spectroscopy" in *Solid State Physics*, edited by F. Seitz and D. Turnbull (Academic Press Inc., New Yerk, 1958), Suppl. 1.

involve time average concerning the torsional oscillation, the time average of the above-mentioned relation must be considered. The time average of field gradient tensor is diagonal and is given by the same Eqs. (1), provided that eQq_0 and η_0 for the stationary molecules are replaced respectively by eQq and η which are

$$eQq=eQq_0\left[1-<\theta_X^2>\frac{3+\eta_0}{2}-<\theta_Y^2>\frac{3-\eta_0}{2}\right], \tag{4}$$

$$\eta=\frac{q_0}{q}\left[\eta_0(1-2<\theta_Z^2>)-<\theta_X^2>\frac{3+\eta_0}{2}+<\theta_Y^2>\frac{3-\eta_0}{2}\right]. \tag{5}$$

The torsional oscillation about Z axis does not affect eQq but acts upon η to decrease it.

The mean energy of each torsional oscillation can be assumed to be equal to the mean energy of corresponding quantum mechanical harmonic oscillation, i.e.[11]

$$<\theta_i^2>=\frac{h}{4\pi^2A_i\omega_i}\left(\frac{1}{2}+\frac{1}{\exp(h\omega_i/kT)-1}\right) \tag{6}$$

where $\omega_i=\omega_X, \omega_Y, \omega_Z$ are the three torsional frequencies, A_i is the corresponding moment of inertia, T the absolute temperature, k the Boltzman's constant and h the Plank's constant.

The distance between two iodine nuclei in a *p*-diiodobenzene molecule has been studied[12] both in gas and solid states by means of electron and X-ray diffractions respectively. Both measurements gave the distance of I-I as 6.85 A, which shows that intermolecular interaction is so weak that *p*-diiodobenzene is certainly in the form of molecular crystal. Therefore q_0 and η_0 can be assumed not to relate with volume or temperature, and the moment of inertia of the molecule, which is to be calculated from the dimension of molecule alone, can be also assumed to be independent on temperature. However, the torsional frequency depends on temperature, for the oscillation is not rigorously harmonic.

Ichishima[13] measured the temperature dependence of low frequency Raman lines in some molecular crystals under constant pressure between liquid air and room

11) H. Eyring, J. Walter and G. E. Kimball: *Quantum Chemistry* (Wiley, New York, 1949). M. Born and K. Huang: *Dynamical Theory of Crystal Lattices* (Clarendon Press, Oxford, 1954).

12) S. B. Hendricks, L. R. Maxwell, V. L. Mosley and M. E. Jefferson: J. Chem. Phys. **1** (1933) 549.

13) I. Ichishima: Rep. Rad. Chem. Res. Inst. (Tokyo Univ.) **4** (1949) 9: J. Chem. Soc. Japan Pure Chem. Sect. **70** (1949) 391, **71** (1950) 332, 366, 443 (in Japanese).

temperatures. The frequency was found to be a linear function of temperature, i.e.

$$\omega_i=\omega_i^0\ (1-g_iT) \tag{7}$$

where T is the absolute temperature and ω_i^0 is the frequency at $T=0$. If the anharmonicity is small, the relation (7) can be used in the formula (6). Then $<\theta_i^2>$ becomes a non-linear function of temperature even in the region where $(h\omega_i/kT)<1$ holds, while in this region, $<\theta_i^2>$ in the formula (6) with a definite ω_i changes linearly with temperature.

For the theory to be consistent with experimental data, there are more factors to be considered. Some intramolecular vibrations of *p*-diiodobenzene should be taken into consideration, while those of chlorine compounds can be neglected owing to the lightness of chlorine atoms. The molecules such as *p*-diiodobenzene have thirty intramolecular vibrations, among which C-I bending vibrations mainly affect the values of eQq and η of iodine. The bending vibrations in and out of molecular plane have the same influence on quadrupole resonance frequencies as $<\theta_X^2>$ and $<\theta_Y^2>$ respectively. Since there are some normal vibrations which have the same influences as $<\theta_Z^2>$, all these effects are summed up in the following formulae,

$$eQq=eQq_0\left[1-\frac{3+\eta_0}{2}\sum_{j=0}^{M}<\theta_{Xj}^2>-\frac{3-\eta_0}{2}\sum_{j=0}^{M}<\theta_{Yj}^2>\right], \tag{8}$$

$$\eta=\frac{q_0}{q}\left[\eta_0(1-2\sum_{j=0}^{M}<\theta_{Zj}^2>)-\frac{3+\eta_0}{2}\sum_{j=0}^{M}<\theta_{Xj}^2>+\frac{3-\eta_0}{2}\sum_{j=0}^{M}<\theta_{Yj}^2>\right], \tag{9}$$

where $j=0$ indicates intermolecular torsional vibrations, i.e. $\theta_{X_0}=\theta_X$, and $j=1, 2, \cdots, M$ indicate intramolecular vibrations. In the above formulae it is presumed that Eq. (6) can be available also for intramolecular vibrations and rewritten as

$$<\theta_{ij}^2>=\frac{h}{4\pi^2A_{ij}\omega_{ij}}\left(\frac{1}{2}+\frac{1}{\exp(h\omega_{ij}/kT)-1}\right). \tag{6'}$$

3. Experimental Procedure and Results

(a) *Pure Quadrupole Resonance*

When thermal vibrations are taken into consideration, two pure nuclear quadrupole resonance frequencies are given in the following equations instead of the formulae (1)

$$\nu_1=\frac{3}{20}eQq\left(1+\frac{59}{54}\eta^2\right), \tag{10}$$

$$\nu_2=\frac{3}{10}\,eQq\left(1-\frac{11}{54}\,\eta^2\right).$$

Here, terms of higher than η^2 are dropped, for η of *p*-diiodobenzene is smaller than 0.1.

The low frequency resonance line of ν_1 of *p*-diiodobenzene was observed by Hatton and Rollin,[14] and by Schawlow[15]. Bray *et al.*[16] measured both high and low resonance frequencies, ν_2 and ν_1, at 77°K and determined the asymmetry parameter, η, as 0.041 ± 0.005. But the data obtained in these experiments are not enough to discuss the temperature variation of eQq and η. It seems necessary to determine accurately the two resonance frequencies, and hence η and eQq, by means of simultaneous measurement[17], because in this method the relation between the two frequencies can be obtained without the use of thermometer or the value of temperature coefficient which is otherwise indispensable.

Apparatus and procedure of experiments were almost similar to those reported previously on solid iodine[17]. Because the asymmetry parameter of *p*-diiodobenzene is so small that the ratio of the two resonance frequencies is almost equal to 1:2, two oscillators for super-regenerative detection of the two resonance frequencies interacted each other. To avoid this interference. oscillation of one of the two oscillators was stopped during the measurement of the other resonance frequency. This procedure made no essential difference from simultaneous measurement, for the interval of the two measurements was quite short owing to the small asymmetry parameter. During the measurements of the two resonance frequencies it was not necessary to recalibrate the frequency meter with a quartz oscillator of 100 kc provided in it, besides, this calibration often wasted much time. The accurate frequency meter which served to determine resonance frequencies on an oscilloscope can give six significant figures of a frequency between 20 Mc and 600 Mc, and in it an oscillator of frequency range between 20 and 30 Mc is provided. One of the difficulties met with precise determination of resonance frequency is concerned in selecting the center of resonance line. This difficulty was removed by the method mentioned in the measurement of solid iodine.[17]

Dr. R. Harada, Department of Chemistry, Faculty of Science, Tokyo University of Education, kindly prepared for the author a highly purified sample. The sample of about 42 g was sealed in a glass tube of 2.5 cm in diameter, 7.5 cm in length.

14) J. Hatton and B. V. Rollin: Trans. Faraday Soc. **50** (1954) 358.
15) A, L. Schawlow: J. Chem. Phys. **22** (1954) 1211.
16) P. J. Bray, R. G. Barnes and R. Bersohn: J. Chem. Phys. **25** (1956) 813.
17) A. Shimauchi: Sci. Light **6** (1957) 58.

Two coils at the ends of a pair of parallel transmission lines from two oscillators are aligned axially and the sample is placed within the coils bridging them. The two oscillators are, one for low and the other for high resonance frequency detection. Transmission lines of the second oscillator were made longer than their normal length by about a half of the wave length of higher resonance frequency for convenience of cooling the sample. The experiments at temperatures below the room temperature were performed in petrolium ether cooled by dry ice and in liquid nitrogen.

Signal-to-noise ratio of the resonance line is about 2 at room temperature; it amounted to 5 at 77°K, for resonance lines became sharper as the temperature was lowered. Therefore the values of eQq and η at 77°K are more accurate than those at room temperature though even the latter values are fairly improved. However, since it is difficult to maintain constant temperature of petrolium ether cooled by dry ice, the data obtained in this condition have more errors than the other.

The observed resonance frequencies at four different temperatures and the constants, eQq and η, calculated by Eqs. (10) are listed in Table 1. It is known that

Table 1. Observed nuclear quadrupole resonance frequencies of I^{127} in *p*-diiodobenzene.

Temperature (°K)	ν_1 (Mc)	ν_2 (Mc)	eQq (Mc)	η
77	280.059	559.056	1864.08	0.038_3
217	278.31	554.44	1852.1	0.04_{05}
285.5	276.854	552.480	1842.24	0.041_4
297.6	276.679	552.107	1841.01	0.041_3

p-diiodobenzene has two phases at room temperature. A phase transition revealed by a volume change has been observed to occur at 50°C,[18] but the nuclear quadrupole resonance observations by Schawlow[15] showed that the high temperature phase can be supercooled down to 20°C at least. In the present work, the sample of single phase was made by recrystallization from solution at room temperature above which it was not heated during the measurement. The values η and eQq estimated this time are plotted against temperature in Fig. 2.

(b) *Raman Effect*

The Raman spectroscopy of crystalline powder is one of interesting subjects in the study of solid state, but is the most difficult branch of spectroscopy. Most of Raman lines peculiar to solid samples are likely to appear in the vicinity of exciting lines. Therefore detection of these lines is difficult and work in this field is scarce.

18) K. Veberreiter and H. J. Orthmann: Z. Naturforsh. 5a (1950) 101.

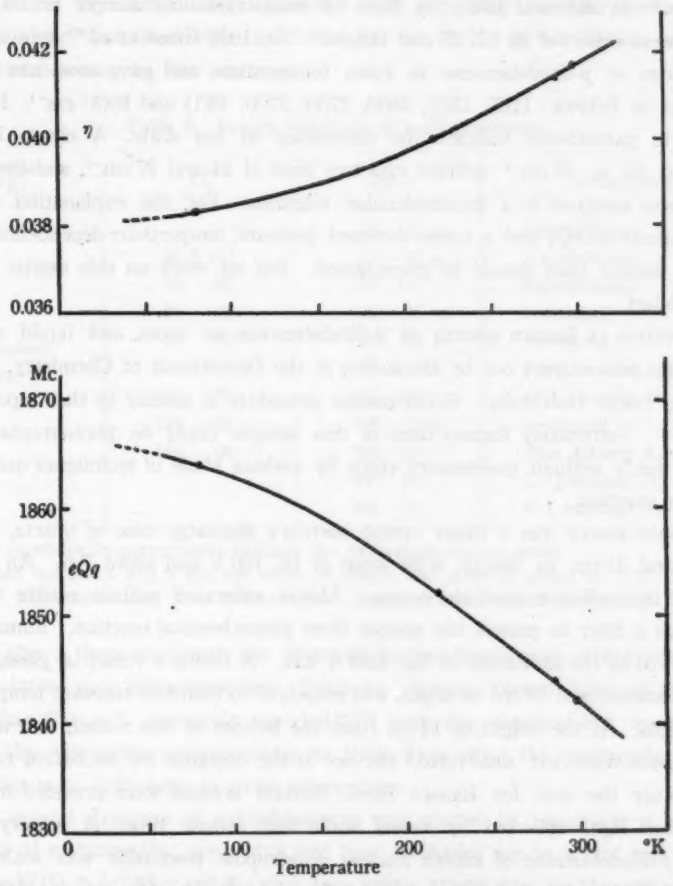

Fig. 2. Temperature *vs.* quadrupole coupling constant eQq and asymmetry parameter η of I^{127} in *p*-diiodobenzene.

In a low frequency region of about 2 to 150 cm^{-1}, some Raman lines peculiar to crystal can be observed. They are distinguished from intramolecular vibrations with line shapes and temperature dependence of these frequencies which can be predicted by thermal expansion. They have strong intensity and fairly broad width. This was observed first by Gross and Vuks in 1935[19].

Low frequency Raman lines of *p*-diiodobenzene were investigated by Gross and

19) E. Gross and M. Vuks: Nature **135** (1935) 100, 431, 998.

Korshunov[20] in 1939 and 1945; the lines of monocrystalline sample at room temperature were observed at 15, 25 and 115 cm^{-1}. In 1950 Gross *et al.*[21] reinvestigated Raman lines of *p*-diiodobenzene at room temperature and gave new data on their frequencies as follows: 11(2), 15(5), 24(8), 27(8), 37(3), 49(1) and 90(3' cm^{-1}, here the numbers in parentheses indicate the intensities on ten scale. A single line first reported to lie at 25 cm^{-1} splitted into two lines of 24 and 27 cm^{-1}, and the line at 115 cm^{-1} was assigned to a intramolecular vibration. For the explanation of temperature effects on eQq and η under constant pressure, temperature dependence of low frequency Raman lines should be investigated. But no work on this matter has yet been published.

Observation of Raman spectra of *p*-diiodobenzene at room and liquid nitrogen temperatures was carried out by the author at the Department of Chemistry, Faculty of Science, Tokyo University. Experimental procedure is similar to that reported by Ichishima.[18] Fortunately Raman lines of this sample could be photographed comparatively easily without preliminary trials by various kinds of techniques needed for some other samples.

The light source was a water cooled mercury discharge tube of quartz, 2 cm in diameter and 15 cm in length, with input of DC 100 V and about 7 A. An electric fan served for cooling around the source. Almost saturated sodium nitrite solution was used as a filter to protect the sample from photochemical reaction. Raman lines were observed by the excitation of Hg 4358 A line. A Dewar's vessel of glass, 4.5 cm in inside-diameter and 50 cm in depth, was employed to maintain constant temperature of the sample. At the height of 12 cm from the bottom of this vessel, two windows of 4 cm square were left unsilvered: the one is the entrance for excitation radiation and the other the exit for Raman lines. Several screens were provided to shield possible stray light reflected by vessel walls and sample tube. A polycrystalline sample of *p*-diiodobenzene of known nuclear quadrupole resonance was sealed in a thin glass cylinder of 2 cm in diameter and 0.8 cm high. A glass spectrograph with two 60° prisms, dispersion of which is about 16 A/mm in 4358 A vicinity, was employed. Suitable exposure on films of Eastman Kodak antihalation 103a-J was 4 to 8 hours. Iron arc lines were photographed as reference standards on all of the films used. Photometric curves of several spectra were traced to determine the positions of Raman lines.

In the experiment at room temperature, the Dewar's vessel was filled with water

20) E. F. Gross and A. V. Korshunov: Compt. rend. acad. sci. URSS **24** (1939) 328: Acta Physicochim. URSS **20** (1945) 353.

21) E. G. Gross, A. V. Korshunov, and V. A. Selkin: Zhur. Eksptl. Teoret. Fiz. **20** (1950) 292.

at 26.5°C, and the sample was immersed in it to minimize temperature variation. When the vessel was filled with liquid nitrogen at 77°K, an air blower served to prevent from dewing on the windows.

Table 2. Raman spectrum of *p*-diiodobenzene.

Temperature (°K)	77	299.5	assignment
Frequency (cm^{-1})		11 (1) a	translational
	15.5 (1)	15 (2) a	translational
	19 (0)	18 (0)	translational
	26 (8)	23 (8) b	rotational
	30 (8)	27 (8) a	rotational
		90 (1) a	(ring bending B_{1u})
	111 (3)	111 (3)	ring bending B_{3g}
	134 (8)	116 (3) b	rotational
	158 (8)	158 (8)	ring deform A_g
		250 (0)	C–I bending B_{1g}
		286 (0)	C–I bending B_{2g}

The numbers in parentheses indicate the intensities on ten scale.
Values marked a and b are the same or nearly the same as given by E. F. Gross, A. V. Korshunov, and Y. A. Selkin: Zhur. Eksptl. Teoret. Fiz. **20** (1950) 292.

In Table 2 there are listed the observed Raman frequencies, which are assigned to both inter- and intra-molecular vibrations. Strong Raman lines of frequencies higher than 600 cm^{-1}, previously reported,[22][23] were also observed but were omitted, because the vibrations corresponding to these lines affect the quadrupole resonance frequencies very little even at room temperature.

The crystal structure of *p*-diiodobenzene was studied by Hendricks *et al.*[12] The crystal is of orthorhombic symmetry and four molecules are in a unit cell of dimensions $a_0=17.00$, $b_0=7.38$, $c_0=6.21$, and the iodine atoms are in the space group of V_h^{15}. From this crystal structure and smallness of intermolecular interactions, approximately three infrared active translational vibrations and three Raman active torsional vibrations are expected.[13]

Generally, Raman lines corresponding to the translatory mode have extremely low frequencies and very weak intensities. *P*-diiodobenzene Raman lines of frequencies 11, 15 and 18 cm^{-1} at room temperature are very weak and their intensity decrease with falling temperature. Some other similar molecular crystals, e. g. benzene

22) O. Paulsen: Monatshefte f. Chem. **72** (1939) 244.
23) Landolt-Börnstein: *Zahlenwerte und Funktionen* (Springer-Verlag, Berlin, 1951) I. Bd., 2 Tl. p. 313.

and *p*-dichlorobenzene which have a center of symmetry and hence their translatory mode are Raman inactive, were found to have a similar characteristic.[23][24] But Ichishima and Mizushima assigned these low frequency lines to translational vibration resulting from invalidation of selection rule by the rise of temperature. The above-mentioned three lines of *p*-diiodobenzene can be interpreted similarly as of translational mode.

Usually rotational oscillations have relatively high frequencies and strong Raman

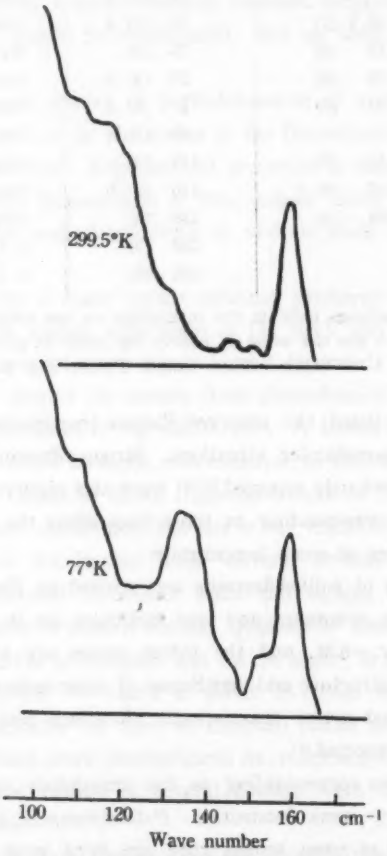

Fig. 3. Photometrically traced temperature dependence of low frequency Raman lines of *p*-diiodobenzene. The upper curve was obtained at room temperature and the lower one at 77°K.

24) I. Ichishima and S. Mizushima: J. Chem. Phys. **18** (1950) 1686, **19** (1951) 388.

lines. In the case of *p*-diiodobenzene, at 77°K strong Raman lines were observed at 26, 30 and 134 cm^{-1}, the first two being almost in equal intensities even at room temperature while their frequencies become 23 and 27 cm^{-1} at 299.5°K respectively. The line at 134 cm^{-1} was sharp and strong at 77°K, but lost its intensity and became diffuse as the temperature was raised. The line width amounted to about 10 cm^{-1} at 299.5°K and its center was estimated to lie at 116 cm^{-1}. Photometrically traced temperature dependence of these Raman lines are shown in Fig. 3. Similar behavior of Raman lines was also observed on *p*-dichlorobenzene by Ichishima.[18] The rotational frequency will naturally depend upon the moment of inertia characteristic of a given mode of oscillation. The frequencies 23 and 27 cm^{-1} at room temperature will represent rotational oscillations about the axes of the largest and intermediate moments of inertia respectively, while the frequency 116 cm^{-1} at room temperature will be of the oscillation about the axis of the smallest moment of inertia, the axis of which is in the plane of molecule and passes through the iodine atoms. The axis of the largest inertia is perpendicular to the plane of the molecule. Since the positions of the halogens are unchanged through a rotation about the axis of the smallest inertia, all of Raman spectra of *p*-dichlorobenzene, *p*-dibromobenzene and *p*-chlorobromobenzene should have in common a line of the same frequency, which was actually observed at 93 cm^{-1} at room temperature. In the spectra of *p*-diiodobenzene, the line at 116 cm^{-1} may correspond to this kind of vibration, since the difference between 93 cm^{-1} and 116 cm^{-1} in frequencies of this order is ascribable to the difference of crystal structures: the former three are monoclinic and the latter is orthorhombic.

To explain the temperature dependence of the nuclear quadrupole resonance frequencies of *p*-dichlorobenzene and the others, intramolecular vibration can often be ignored owing to its high frequency. But in the case of *p*-diiodobenzene some intramolecular vibrations have such low frequencies that they can not be neglected. *P*-diiodobenzene molecule itself has the symmetry V_h. According to the "Table of characters of the group V_h symmetry species" by Herzberg[25] or Wilson *et al.*[26] the normal intramolecular vibrations devide themselves into symmetry species as follows;[27]

$$6A_g+5B_{1g}+1B_{2g}+3B_{3g}+2A_u+3B_{1u}+5B_{2u}+5B_{3u}\,.$$

---

25) G. Herzberg: *Molecular Spectra and Molecular Structure* Vol. II *Infrared and Raman Spectra* (D. Van Nostrand Co. Inc., New York 1945).

26) E.B. Wilson, Jr., J.C. Decius and P.C. Cross: *Molecular Vibrations* (McGraw-Hill Book Co. Inc., New York 1955).

27) Here the designation of symmetry species follow Herzberg's, while there is another designation, namely $B_{1g} \rightleftarrows B_{2g}$, $B_{1u} \rightleftarrows B_{2u}$.

In this case the directions of x, y, and z axes are different from the principal axes employed in Chapter 2: y and z axes refer respectively to I–I direction and perpendicular to the molecular plane. Namely the relation between the two axial systems can be given as $Z=y$, $Y=x$ and $X=z$. The vibrations of all of g species are Raman active and species B_{1u}, B_{2u} and B_{3u} vibrations are infrared active. The two vibrations of species A_u are inactive in both Raman and infrared spectra.

Among molecules similar to *p*-diiodobenzene molecule, those of *p*-dideuterobenzene[28] and *p*-difluorobenzene[28] were so thoroughly investigated that all the frequencies of their normal vibrations were worked out and some of them were confirmed by experiments. As for *p*-dichlorobenzene and *p*-dibromobenzene, most of high frequency vibrations were assigned.[29] On *p*-diiodobenzene, nine intramolecular vibrations of frequencies higher than 600 cm^{-1} have so far been reported.[23] In this work, the low frequency intramolecular vibrations were observed for the first time. By comparing the molecule of *p*-diiodobenzene with the above-mentioned similar molecules, the obtained data were analysed as follows.

606 cm^{-1} E_{2g} vibration in benzene is split into A_g and B_{1g} vibrations in *p*-diiodobenzene, and most reasonable assignment seems to be $A_g=158$ cm^{-1} and $B_{1g}=624$ cm^{-1}. These vibrations may be roughly characterized by ring deformation mode. The observed line at 250 cm^{-1} may be assigned to one iodine bending vibration in the molecular plane, B_{1g}, which is Raman active and probably originated chiefly from E_{2g} and A_{2g} of benzene. The three nonplanar vibrations of species B_{3g} may be designated approximately as one ring bending, one iodine bending, and one hydrogen bending modes. The lowest B_{3g} fundamental, i.e. ring bending, is the medium intensity Raman line at 111 cm^{-1}, and intermediate frequency of this species, i e. iodine bending, is assigned to the weak line at 286 cm^{-1}.

(c) *Far-Infrared Absorption*

The absorption spectrum of *p*-diiodobenzene in far-infrared (200 cm^{-1}—50 cm^{-1}) was studied, because several infrared active vibrations were expected to be of low frequencies as revealed by Raman spectroscopy.

The experiments were performed at the Department of Applied Physics, Faculty of Engineering, Osaka University, where a far-infrared spectrograph had been instal-

---

28) E. E. Fergnson, R. L. Hudson, J. R. Nielsen and D. C. Smith: J. Chem. Phys. **21** (1953) 1457.
A. H. Delsemme: J. Chem. Phys. **18** (1950) 1680.

29) K. W. F. Kohlrausch: Phys. Z. **37** (1936) 58.
H. Sponer and J. S. Kirby-Smith: J. Chem. Phys. **9** (1941) 667.
G. Nordheim and H. Sponer: J. Chem. Phys. **11** (1943) 253.
See p. 70–71 in ref. 23.

led several years ago[30]. This spectrograph of Czerny-Turner type is reported to have resolving power of about 0.5–0.3 cm^{-1} over the region from 18 μ to 1000 μ.

Usually powdered sample is mixed with polyethylene to make a thin plate, which is placed inside the spectrograph. The spectrograph is then evacuated. This procedure was given up because *p*-diiodobenzene easily sublimates. The powdered sample used was first kneaded with nujol to make paste, which was then tightly sandwiched between two polyethylene plates kept apart by a thin polyethylene frame. The size of the polyethylene window was 2.5×7.3 cm, and the thickness of sample was about 1 mm. The sample thus treated was set outside the entrance slit where usually a gas cell of almost 20 cm path length is placed. Thus the incident radiation was made to pass through about 20 cm length of free air.

The whole investigated region (50–200 cm^{-1}) was divided into five spectral regions, 50–58, 58–90, 90–115, 115–150 and 150–200 cm^{-1}. In the first two regions echellete grating of 80 lines/inch, and in the last three regions that of 160 lines/inch were used. Different sets of filters were used in each of five ranges. The radiation source was a high pressure mercury lamp and the detector was a Goley cell.

The estimated transmission curve is shown in Fig. 4, on which three weak absorptions at about 90, 111 and 158 cm^{-1}, and a strong absorption at 143 cm^{-1} will

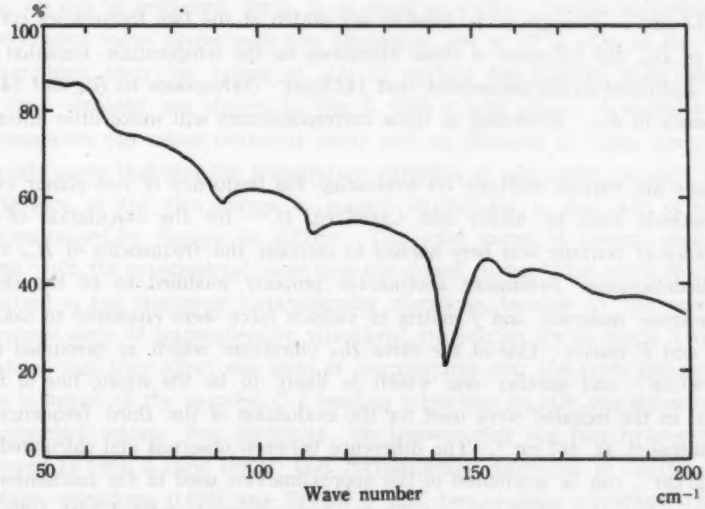

Fig. 4. Far-infrared transmission curve of *p*-diiodobenzene crystal *vs.* wave number.

30) H. Yoshinaga, S. Fujita, S. Minami, A. Mitsuishi, R. A. Oetjen, and Y. Yamada: J. Opt. Soc. Am. 48 (1958) 315.

be noticed. The line in the vicinity of 90 cm^{-1} could not be accurately measured owing to the absorption of water vapor in air in the path. The weak line 111 cm^{-1} seems to correspond to the vibration which is intrinsically infrared inactive but Raman active because of invalidation of rigorous selection rule caused by the molecule having lost its perfect V_h symmetry. The weak line at 158 cm^{-1} seems to be of this kind. Namely it is possibly one of A_g species vibrations which are originally to be only Raman active. Among thirteen infrared active vibrations of *p*-diiodobenzene $3B_{1u}+5B_{2u}+5B_{3u}$, the following three are expected to have low frequencies:

B_{3u} C–I bending in molecular plane

B_{1u} C–I bending out-of-molecular-plane

B_{1u} C–C–C ring vibration of out-of-plane.

The lowest of B_{3u} fundamental is presumed to be the sharp band observed at 143 cm^{-1}. As for B_{1u} C–C–C ring vibration, since it ought to be of low frequency, it is assigned to the line at 90 cm^{-1}. The remaining B_{1u} C–I bending out-of-molecular-plane vibration ought to appear with strong intensity in the investigated region, but no line other than the above-mentioned could be found. Detailed examination of 143 cm^{-1} line gives that it is comparatively wide and the line shape is a little asymmetric. Therefore this line is presumed to be composed of two lines with slightly different frequencies. The centers of these two lines were estimated to lie at 143.0 and 145.7 cm^{-1}. Though it is hard to say which of the two frequencies correspond to B_{1u} or B_{3u}, the influence of these vibrations on the temperature variation of eQq will be estimated on the assumption that 143.0 cm^{-1} corresponds to B_{1u} and 145.7 cm^{-1} corresponds to B_{3u}. Reversing of these correspondences will make little difference to eQq.

There are various methods for evaluating the frequency of non-planar vibration. The methods used by Miller and Crawford, Jr.[31] for the calculation of normal frequencies of benzene was here applied to estimate the frequencies of B_{1u} vibration of *p*-diiodobenzene. Symmetry coordinates properly modified to fit the case of *p*-diiodobenzene molecule and f matrix of valence force were employed to calculate G matrix and F matrix. One of the three B_{1u} vibrations which is presumed to be of about 90 cm^{-1} and another one which is likely to be the strong line at 801 cm^{-1} observed in the infrared were used for the evaluation of the third frequency which was estimated at 167 cm^{-1}. The difference between observed and calculated values, about 23 cm^{-1}, can be attributed to the approximations used in the calculation: some F matrix elements, which do not involve force constants related with iodine atoms were assumed to be identical with those of benzene; iodine and hydrogen bendings

31) F. A. Miller and B. L. Crawford, Jr.: J. Chem. Phys. **14** (1946) 282,

are assumed to have the same influence on the out-of-plane ring-bending motion.

4. Discussion

With the use of experimental results of this work, values of eQq and η were estimated in the following manner. The data obtained by X-ray and electron diffractions,[12] $(2.00\,\text{A})_{\text{I-C}}$, $(1\,42\,\text{A})_{\text{C-C}}$, and $(1.12\,\text{A})_{\text{H-C}}$, served to estimate moments of inertia. A_X and A_Y are almost equal, while A_Z is far smaller: $A_X=5228$, $A_Y=5075$ and $A_Z=153\times10^{-40}$ g cm^2. From the values obtained by Raman spectroscopy the following formulae were derived to evaluate the frequencies of torsional vibration at various temperature.

$$\begin{aligned}\omega_X&=c\cdot27\ (1-0.00050\ T),\\ \omega_Y&=c\cdot31\ (1-0.00043\ T),\\ \omega_Z&=c\cdot140.2\ (1-0.00058\ T),\end{aligned}\qquad(11)$$

c ; light velocity cm/sec,

T ; absolute temperature.

The value of eQq of equation (4) is to be calculated with the use of $\langle\theta_i^2\rangle$ $(i=X, Y, Z)$ of Eq. (6), in which the evaluated ω_i at various temperatures were applied. η_0 in Eq. (4) can be neglected, for η_0 is so small as $\eta<0.1$. On the supposition that the experimental value agrees with the theoretical one at 77°K, eQq_0 of Eq. (4) was first determined, then the values of eQq at various temperature were calculated. Values thus obtained are shown in Fig. 5 with a solid curve. A dotted curve in Fig. 5 represents the values evaluated solely with ω_i obtained at room temperature, namely this curve indicates the temperature variation of eQq under constant volume. The difference of the two curves is mainly attributable to the shift of torsional frequencies caused by change in volume. The solid curve is nearer, though not coincident with, the experimental value than the dotted curve. This small discrepancy was ascribed to low frequency intramolecular vibrations, because in the case of *p*-diiodobenzene some of intramolecular vibrational frequencies are so much lowered by iodine atoms that they affect eQq even at temperatures near the room temperature.

The influence of the so-called C–I bending vibrations on eQq was estimated with newly observed values. For simplicity, the benzene ring and four hydrogen atoms are assumed to form a rigid body,[3] and corresponding moments of inertia of two out-of-plane vibrations (143.0 and 286 cm^{-1}) and two in-plane vibrations (145.7 and 250 cm^{-1}) were obtained. Since the above mentioned four vibration frequencies are probably independent of temperature, values of $\langle\theta_{ij}^2\rangle$ of Eq. (6′) $(i=X, Y;\ j=1, 2)$ were calculated by the use of ω_{ij} at room temperature and corresponding moments

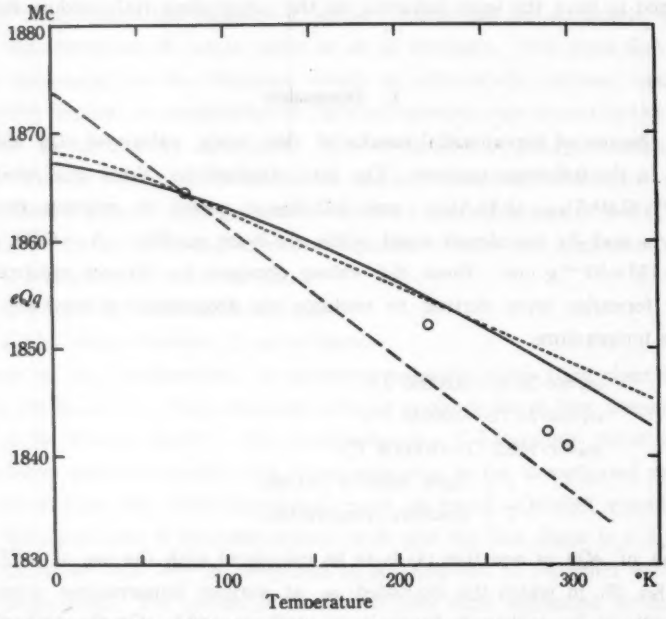

Fig. 5. Temperature variation of the quadrupole coupling constant. Circles are observed values, and curves are by the theory including the effect of torsional oscillations: dotted curve is without and solid curve is with the effect of temperature variation of torsional frequencies. Dashed curve was calculated on the assumption that $\omega_X = 15\,\mathrm{cm}^{-1}$ and $\omega_Y = 25\,\mathrm{cm}^{-1}$ correspond to torsional frequencies.

of inertia obtained above. $\langle\theta_{ij}^2\rangle$ thus estimated and $\langle\theta_{i_0}^2\rangle$ of temperature dependent intermolecular torsional oscillation were used in Eq. (8) to evaluate eQq. The obtained eQq values approach to experimental data as shown in Fig. 6. The agreement to this extent suggests that, at least in the case of eQq, the previously postulated assumptions actually hold, and further some intramolecular vibrations really contribute to the temperature variation. The dotted curve in Fig. 6 was obtained with ω_i at room temperature. The dotted curve involves the effect of intramolecular vibrations in the same way as does the solid curve.

The torsional motion about Z axis does not affect eQq; it contributes to the temperature dependence of resonance frequencies through η alone. The Raman line corresponding to torsional motion about Z axis of *p*-diiodobenzene was sharp at low temperature but diffuse at room temperature. The effect of this torsional oscillation on quadrupole resonance frequencies is small owing to small η, however, rough estimation shows that an uncertainty of $10\,\mathrm{cm}^{-1}$ in Raman line frequency induces

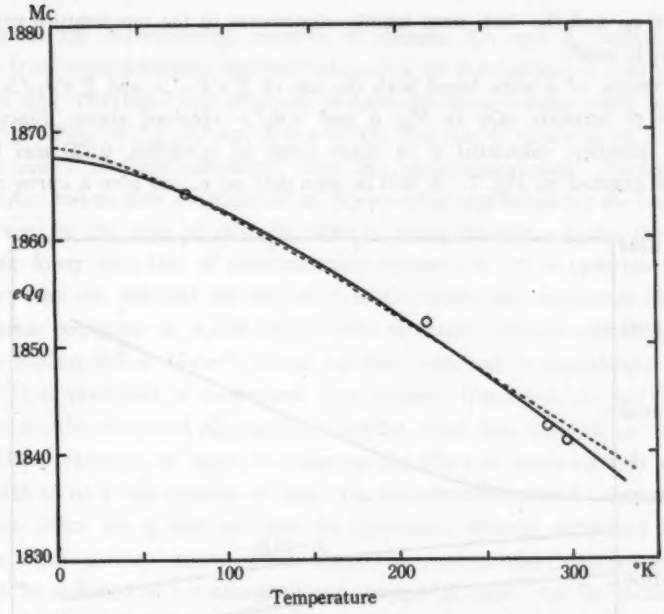

Fig. 6. Temperature variation of the quadrupole coupling constant. Circles are observed values, and curves are by the theory including the effect of intramolecular C–I bending vibrations besides the temperature variation of intermolecular torsional oscillation: dotted curve is without and solid curve is with the temperature variation of torsional frequencies.

several kc uncertainty in ν_1 and ν_2. This may be the cause of small signal-to-noise ratio of resonance lines at room temperature. Among the intramolecular vibrations, which have the same effect as that of intermolecular torsional motion about Z axis, the lowest frequency mode A_u, which is inactive both in Raman and infrared, was estimated to have frequency 402 cm^{-1} by the method discribed in Chapter 3 (c). Therefore its effect on η can be neglected.

Eq. (9) can be changed into the following form

$$\eta=\frac{q_0}{q}\left[\eta_0\left(1-2\langle\theta_z^2\rangle-\frac{1}{2}\sum_j\langle\theta_{xj}^2\rangle-\frac{1}{2}\sum_j\langle\theta_{rj}^2\rangle\right)\right.$$
$$\left.+\frac{3}{2}\left(\sum_j\langle\theta_{rj}^2\rangle-\sum_j\langle\theta_{xj}^2\rangle\right)\right]. \qquad (12)$$

Here the value of q_0/q is calculated by Eq. (8). As η_0 in Eq. (8) can be neglected because of smallness, the second term of the right side of Eq. (12) becomes inde-

pendent of η_0, and the last term mainly contributes to the temperature variation of η when η_0 is small.

The values of η were found with the use of $\sum<\theta_{Xj}^2>$ and $\sum<\theta_{Yj}^2>$ obtained previously to estimate eQq in Fig. 6 and $<\theta_Z^2>$ obtained above. Since η_0 is an uncertain quantity, calculated η in three cases of $\eta_0=0.035$, 0.036 and 0.037 are tentatively graphed on Fig. 7. It will be seen that no η_0 can give a curve consistent

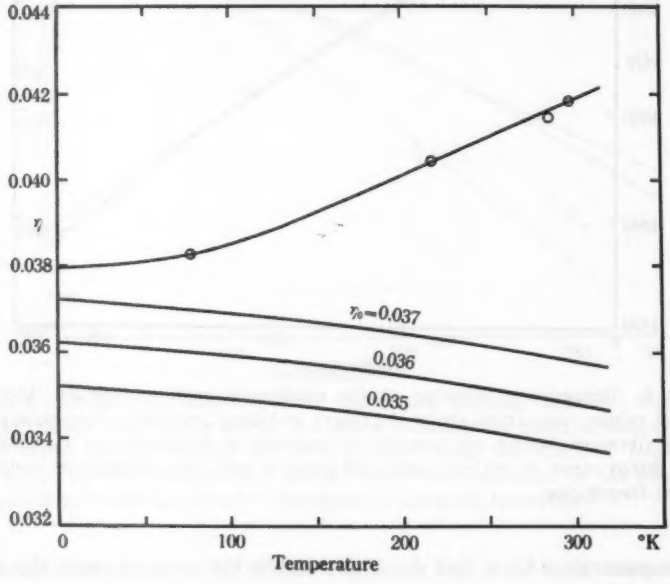

Fig. 7. Temperature variation of asymmetry parameter. Circles are observed values. Lower curves were calculated by Eq. (12) in three cases of $\eta_0=0.035$, 0.036 and 0.037. Upper curve which passes over all the circles was calculated by Eq. (12) with addition of two terms representing the effects of two ring bending vibrations; $\eta_0=0.0361$ and $A_{Yj}=526.3\times10^{-40}$ g cm^2 were assumed.

with experimental values shown with circles. Since the first term of Eq. (12) decreases with temperature, evaluated η can not approach to observed values unless $\sum<\theta_{Yj}^2>$ in the second term is sufficiently large. This seems to suggest that previously mentioned two non-planar ring vibrations, B_{1u}(90 cm^{-1}) and B_{2g}(111 cm^{-1}), should be taken into consideration. This vibration involves some components of C–I bending, magnitude of which can be estimated by that of corresponding moment of inertia. However, it can not be obtained without tedeous calculations, and the estimated value does not always agree with observed.

Therefore the corresponding moment of inertia, A_{rf} and η_0 were tentatively estimated from experimentally obtained values of η by the method of trial and error. If the two ring vibrations are assumed to have the same corresponding moment of inertia $A_{rf}=526.3\times10^{-40}$ g cm^2 and if $\eta_0=0.0361$, the curve obtained by calculation shown in Fig. 7 becomes consistent with the experimental data. Therefore these values of A_{rf} and η_0 may be regarded as representing approximately the true values.

However, in the case of eQq, the effect of these vibrations makes the value of eQq become lower than that of experimentally determined. It is probable that this discrepancy can be canceled by the effect of C–I stretching component of inplanar ring vibration belonging to A_g(158 cm^{-1}). This vibration scarecely affects η.

If the Raman line at 15 cm^{-1}, which has been assigned to translatory mode in Chaptcr 3(b), is presumed to correspond to a torsional frequency, ω_X, and 25 cm^{-1} is adopted as ω_Y, the evaluated eQq becomes smaller than the observed as shown in Fig. 5. There remains no room to take up the effect of intramolecular vibrations which ought to be a fair amount on eQq. On the above-mentioned assumption, the temperature effect on η can not also be illustrated without supposing that ring vibrations affect η very much. From these two reasons, the frequency of 15 cm^{-1} can hardly be assigned to a torsional motion around X axis. As for *p*-dichlorobenzene, Saksena's data[32] on Raman lines are often used as the measured values of torsional vibrations, i.e. $\omega_X=27$, $\omega_Y=54$ and $\omega_Z=93$ cm^{-1}. But with these values, evaluated eQq was reported to be smaller than the observed.[10] Therefore Ichishima's assignment[13] seems more reasonable, with which 27 cm^{-1} corresponds to translatory mode and torsional vibrations correspond to $\omega_X=47$, $\omega_Y=53$ and $\omega_Z=94$ cm^{-1}, since 27 cm^{-1} frequency in *p*-dichlorobenzene possibly corresponds to 15 cm^{-1} frequency of *p*-diiodobenzene.

5. Conclusion

The following experiments were performed with polycrystalline powdered sample of *p*-diiodobenzene.

i) Two quadrupole resonance frequencies of I^{127} nucleus were determined between liquid nitrogen and room temperatures by simultaneous measurement, and temperature dependence of eQq and η were estimated.

(ii) Temperature variations of low frequency Raman lines were investigated and frequencies of torsional oscillations were determined as shown below:

$\omega_X=23$, $\omega_Y=27$ and $\omega_Z=116$ cm^{-1} at 26.5°C changed

to $\omega_X=26$, $\omega_Y=30$ and $\omega_Z=134$ cm^{-1} at 77°K.

32) B. D. Saksena: J. Chem. Phys. **18** (1950) 1653.

The line corresponding to ω_z was diffuse at 26.5°C, but sharp and strong at 77°K.

(iii) Some intramolecular vibrations of low frequencies, which may contribute to eQq and η, were analysed by Raman and far-infrared spectroscopy.

Since *p*-diiodobenzene forms molecular crystal, only the frequencies of torsional oscillations may depend on volume; eQq and η are possibly independent of volume. On this assumption, experimental results were used in the formulae expressing the temperature dependence of eQq and η under constant volume, and the following conclusions were obtained.

(1) When the temperature shift of the frequencies of two torsional oscillations, which affect eQq, are taken into account, calculated values of eQq approach to observed.

(2) Torsional oscillation about I–I axis contributes to resonance frequencies through η. Since the Raman line corresponding to this oscillation is broad at 26.5°C, uncertainty of this frequency may be the cause of small signal-to-noise ratio of resonance frequencies at room temperature.

(3) When the effects of two planar and two non-planar vibratlons are added, temperature dependence of eQq is explained almost completely.

(4) For the explanation of temperature dependence of η, intramolecular vibrations of out-of-plane ring bending, B_{1u} and B_{2g}, besides all the other vibrations mentioned above should be also taken into consideration. The reason why the temperature dependence of eQq is explained without considering the effect of these vibrations is that the effect is probably cancelled by the effect of C–I stretching component of in-planar ring vibration belonging to A_g which scarcely affects η.

(5) When the Raman lines around 15 cm^{-1} are assigned to torsional frequencies, their effects on both η and eQq become too large to explain experimental results. Therefore those lines seem to be of translatory mode appearing as if Raman active due to invalidation of selection rule. This is an example of useful information on assignment of Raman lines being obtainable by the investigation of temperature dependence of pure quadrupole resonance.

6. Acknowledgements

The author wishes to express his sincere thanks to Prof. Shoji Kojima of Tokyo University of Education and Prof. Haruo Ootuka, Director of the Institute for Optical Research, for valuable discussion and encouragement throughout this work, to Prof. Takehiko Shimanouchi of Tokyo University for valuable discussion and letting the author work on Raman spectra in his laboratory, to Dr. Saburo Takeda for co-operation in experimental work, to Prof. Hiroshi Yoshinaga of Osaka University for his kindness, to Dr. Akiyoshi Mitsuishi for helping the author in far-infrared absorption work and to Dr. Rokuro Harada for preparing highly pure sample.

Stydy on [OI]-λ5577 of Night Airglow (I)
—Height of [OI]-λ5577 Emitting Layer—

Noboru ŌTI

Laboratory of Physics, Gifu University, Nagara, Gifu, Japan

(Received April 3, 1961)

Abstract

The height of the layer that emits night airglow is being determined directly from observed values of spectral line intensities. This method, however, involves various errors. A new method is proposed in which values of $R'(z,t)=\overline{R}(z,t)/R(z)$ obtained at two observing stations are used. In this expression, $R(z,t)$ is the observed airglow intensity at zenith distance z and at time t, and $\overline{R}(z)$ is its value averaged over the whole night. This method gives fairly accurate results. The mean of the height thus obtained is 100 ± 23 km.

1. Introduction

Information on particulars of night airglow, especially the height of the layer that glows, is of great import for the study of upper atmosphere. But, as the airglow, the ethereal illuminant that spreads faintly all over the sky, has no definite form and is weak in intensity, the height of its emitting layer can not be determined from measurement of parallax.

The customary method of determining the height by observation made at one station is based on the assumption that the emitting layer is spread horizontally over a fairly wide area with uniform thickness and uniform specific intensity of glow so that the intensity in one direction should become proportional to path length of the layer measured in that direction and hence the rate of increase in intensity by the increase of zenith distance should determine the height of the layer (Fig. 1).

From this reasoning, van Rhijn[1] gave the intensity $I(z)$ at zenith distance z as

$$I(z)=\frac{I_0}{\sqrt{1-\left(\frac{R}{R+h}\sin z\right)^2}}$$

where I_0 is the intensity at the zenith, h is the height of the emitting layer and R is the radius of the earth.

1) P. J. Van Rhijn: Bull. Astron. Inst. Metherlands **2** (1924) 75.

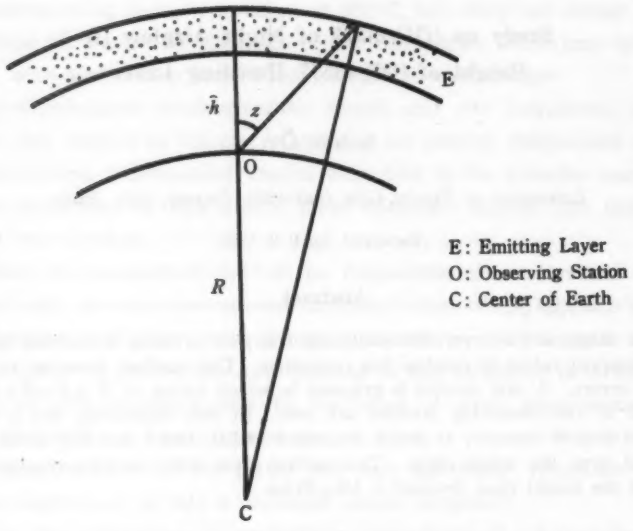

Fig. 1. Principle of height measurement by observation at one station.

At present, as the knowledge on airglow intensity is fairly well advanced, we know that this way of measuring the height involves many errors. The chief cause of error is the assumption that the night airglow is calm and almost uniformly distributed over a wide region. Successive observations showed that the airglow intensity varies very much both with position and with time. In relation to this, extinction of light in the atmosphere is difficult to be evaluated. Up to the present, therefore, only a rough estimation of the height has been made. In short, the measuring of the height by observation made at one station is not commendable.

Other methods[2)3)] of measuring the height have since been devised by utilizing the variation of airglow intensity with position and time and by taking uninterrupted photometric records of intensity distribution of the glow over the whole sky at two chosen stations from where the same region of the glow can simultaneously be observed. On these records, the region of the glow that was ascertained to have been observed by the two stations in common is picked up, and its height is found trigonometrically. But the uncertainty of the value of light extinction coefficient of the atmosphere still persists besides other sources of error causing considerable

2) M. Huruhata, H. Tanabe and T. Nakamura: Rep. Ionosphere Res. Japan **9** (1755) 144.
3) F. E. Roach, D. R. Williams, P. St. Among, H. B. Pettit add R. G. Weldon: Ann. Astrophys. **17** (1954) 172.

inaccuracy of the measurement.

By the author's new way of treating the data obtained at two stations, accuracy of measurement was enhanced.

2. Method of Measurement

Determination of the height of airglow layer by simultaneous observations at two stations should be possible if the variation of glow intensity with time and position is based upon as explained above, provided that the measuring apparatus and recorders used at the two stations are of the same types or properly standardized and the extinction coefficient of atmosphere of the two localities is correctly known. These conditions are however not easily fulfilled; some inevitable error is introduced into the determination. The relation of the observed value $R(z, t)$ to its true value $I(z, t)$ may be expressed as

$$R(z, t)=K(z)\ \{I(z, t)+C(z)\} \tag{2.1}$$

where $K(z)$ represents the extinction effect of atmosphere and $C(z)$ is the error mainly due to inaccuracy in estimating the effect of background light. This means that the deviation of observed value from true value is not to be ignored. $C(z)$ may be regarded as a constant of the apparatus if z is fixed, and as it is unlikely that $C(z)$ varies considerably with z, we may put $C(z)$=const. The term $K(z)$ may be a constant all through night, but it may vary from night to night, and its measurement is quite difficult as described before. However, as for the effects of $K(z)$ and $C(z)$ on $R(z, t)$, it is shown that the influence of $K(z)C(z)$ is less than about 10 per cent of that of $K(z)I(z, t)$. Regarding $K(z)$ as the sole origin of errors concerning $R(z, t)$, we can rewrite the expression (2.1) as

$$R(z, t)=K(z)I(z, t)\,. \tag{2.2}$$

Averaging this expression over the whole night, we have

$$\bar{R}(z, t)=K(z)\bar{I}(z, t)\,. \tag{2.2}'$$

Using the expressions (2.2) and (2.2)′, we define a quantity $R'(z, t)$ as follows:

$$\frac{R(z, t)}{\bar{R}(z, t)}=\frac{K(z)}{\bar{K}(z)}\,\frac{I(z, t)}{\bar{I}(z, t)}=\frac{I(z, t)}{\bar{I}(z, t)}=R'(z, t)\,. \tag{2.3}$$

Then, $R'(z, t)$ is independent of $K(z)$, and it will be seen that reliable results with little errors can be obtained by using this quantity $R'(z, t)$. We now proceed to describe this method.

Suppose two points P_A and P_B in the emitting layer, and assume that both the

zenith distance of P_A at station A and that of P_B at station B are z_1. Let z_A be the zenith distance of P_B when seen from station A, and similarly, Z_B be the zenith distance of P_A seen from station B. If the heights of P_A and P_B are equal, we put $z_A=z_B(=z_2)$. (Fig. 2) Hereafter we shall use $R'(z,t)$ to examine the relations between observed values at station A and those at station B, because, whereas $R(z,t)$ involves various kinds of errors, $R'(z,t)$ is free from such ambiguity. Then, the relations between the values $R_A'(z_1,t)$ of P_A obtained at station A and the values $R_B'(z_1,t)$ of P_B obtained at station B must be the same as the relations between the values $R_A'(z_2,t)$ of P_A obtained at station B and the values $R_B'(z_2,t)$ of P_B obtained at station A.

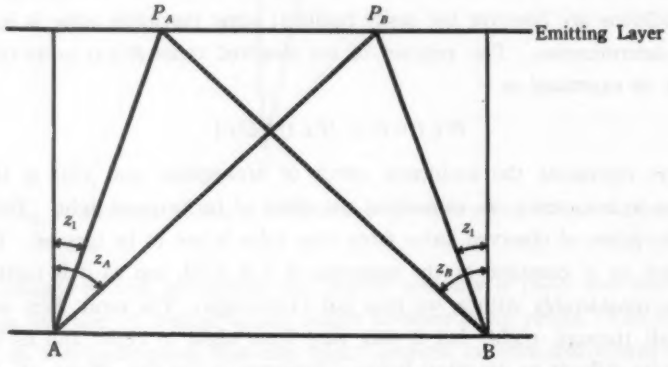

Fig. 2. Principle of height measurement by observations at two stations.

Hence, if we can find somehow or other, from the data obtained at the two stations, two zenith distances z_1 and z_2 which satisfy the condition that the relations between $R_A'(z_1,t)$ and $R_B'(z_1,t)$ are the same as the relations between $R_A'(z_2,t)$ and $R_B'(z_2,t)$ we can calculate the height h by the following expression,

$$h=\frac{D}{\tan z_1+\tan z_2} \tag{2.4}$$

where D is the distance between A and B.

Various expressions may be used to represent the relations between $R_A'(z,t)$ and $R_B'(z,t)$, but the most convenient quantity for the statistical treatment is δ_z defined by

$$\delta_z=\sqrt{\sum\{R'(z,t)-R'(z,t)\}^2/N} \tag{2.5}$$

where N is the number of observations through the night. Thus, if we can find z_1

and z_2 which make δ_{z_1} equal to δ_{z_2}, h can be calculated by the procedure described above.

Next, from the same consideration, another expression $r(z)$ may also be used to find z_1 and z_2 which is

$$r(z)=\sqrt{\sum\left\{\frac{R_A'(z_1,t)}{R_B'(z_1,t)}-\frac{R_B'(z_2,t)}{R_A'(z_2,t)}\right\}^2/N}. \tag{2.6}$$

This implies that, if z_1 and z_2 are the zenith distances at which the same region of the emitting layer is observed from the two station, $r(z)$ should become zero. Actually, it is not zero on account of various involved errors, nevertheless, if we find the values of z_1 and z_2 which make $r(z)$ minimu, h can be computed from Eq. (2.4).

3. Observations and Discussions

An observing station was set up at Gifu (CSAGI No. C167) to comply with the cooperative observation system during the periods of the IGY and IGC to study the emission line [OI]-λ5577 of airglow with a photoelectric photometer. As for the geographycal relations, the station at Sendai is located exactly north-east of the station at Gifu with the distance of 430 km in between. This is a very favourable situation for our pourpose as will be seen later.

At Sendai, observation on the emission line [OI]-λ5577 was made with the same apparatus as used in Gifu.

Performance of the automatic photometer used for this investigation is as follows: the photometer changes its direction successively to sixteen aximuths from north with equal intervals during one rotation, stopping for one and half minutes automatically at every azimuth. While stopping, it is directed successively to six altitudes from zenith, these six zenith distances being 0°, 33.7°, 53.1°, 63.4°, 69.4° and 75.0°. Thus the photometer scans automatically 96 points over the whole sky for 24 minutes. As mentioned above, NE azimuth direction at Gifu and SW azimuth direction at Sendai happen to be on one straight line. During the IGY, many observing stations in Japan reported[4] the airglow intensities in all azimnths in half an hour intervals. There are four days on which Gifu and Sendai stations recorded [OI]-λ5577 line intensity simultaneously for over five hours. From these records the values of δ_z were calculated to find z_1 and z_2, with which the height h of the layer could be computed. The results are shown in Table 1.

Beside aforementioned $K(z)$ and $C(z)$, we can not but admit the error of around

4) National Committee for IGY "Absolute intensity of Night Airglow (5577) during IGY" Dec. (1959).

3 per cent on the values of $R(z, t)$ arising from photomultiplier noise and reading of photometer records. Therefore, even if we assume that the distribution of observed values of $R(z, t)$ around their mean value follows the law of probability and that the deviation is not too large when the restricted number of observation is considered, error of about one per cent on calculated values of δz is unavoidable.

With due consideration on these errors, every pair of z_1 and z_2, which is used for the calculation of respective layer height by (2.4), was presumed from the data given in Table 1 and is shown in Table 2 together with the values of height h calculated by (2.4).

Table 1. δ_z values (Calculated from over five hours simultaneous observation data obtained at Gifu and Sendai stations) ($\times 10^{-2}$).

Date			Zenith distance 33.7°	53.1°	63.4°	69.4°	75.0°
57	Oct.	23/24	9.42	9.28	7.08	5.51	6.96
	Nov.	22/23	9.17	5.79	5.62	7.02	—
58	Oct.	16/17	11.38	10.32	4.89	4.07	8.12
	Dec.	13/14	11.91	7.62	6.64	7.65	14.05

Table 2. z_1 and z_2 which are used to compute the height h by (2.4) and the obtained values of h.

Date			z and h z_1	z_2	h(km)
57	Oct.	23/24	63.4°	75.0°	76
	Nov.	22/23	53.1°	63.4°	127
58	Oct.	16/17	63.4°	69.4°	89
	Dec.	13/14	53.1°	69.4°	109

From the values of h of the four days shown in Table 2, we obtain for the mean value of h

$$h = 100 \pm 21 \text{ km}.$$

Next, pairs of z_1 and z_2 which are obtained from (2.6) are shown in the Table 3. The results agree well enough with the results obtained by using δ_z.

The average value of 100 km thus obtained is in good agreement with the height obtained theoretically by Chapman.[5]

It also coincides well with the height reported by Hepner and Meredith[6] who

5) S. Chapman: Astrophys. J. **91** (1931) 309.
6) J. P. Heppner and L. H. Mereedith: J. Geophys. Res. **63** (1958) 51.

Table 3. $r(z)$ values ($\times 10^{-2}$), and pairs of z_1 and z_2 which make $r(z)$ minimum.

57 Oct. 23/24

z_2 \ z_1	53.1°	63.4°	69.4°	75.0°	a pair of z_1 and z_2
33.7°	16.2	13.6	13.4	12.2	
53.1°		13.6	11.0	12.9	63.4°
63.4°			11.8	**10.5**	75.0°
69.4°				11.5	

57 Nov. 22/23

z_2 \ z_1	53.1°	63.4°	69.4°	75.0°	a pair of z_1 and z_2
33.7°	14.3	12.2	14.0		
53.1°		**9.5**	12.2		63.4°
63.4°			12.5		53.1°

58 Oct. 16/17

z_2 \ z_1	53.1°	63.4°	69.4°	75.0°	a pair of z_1 and z_2
33.7°	22.0	17.9	14.6	16.2	
53.1°		17.0	14.7	10.6	69.4°
63.4°			**9.9**	10.3	63.4°
69.4°				12.4	

58 Dec. 13/14

z_2 \ z_1	53.1°	63.4°	69.4°	75.0°	a pair of z_1 and z_2
33.7°	14.2	16.8	11.0	12.6	
53.1°		8.4	**8.1**	9.5	69.4°
63.4°			8.5	13.7	53.1°
69.4°				14.9	

determined it by rocket observation. (Fig. 3)

It is seen from Table 2 that the height is somewhat lower in October than in other months of the year. While studying the seasonal variation of airglow intensity, the author found that the intensity is especially strong in October. There is perhaps a close relation between the airglow intensity and the height of emitting layer.

In the above calculations, the height is assumed to remain the same all through the night. But if the over-all intensity of the sky undergoes regular fluctuations,

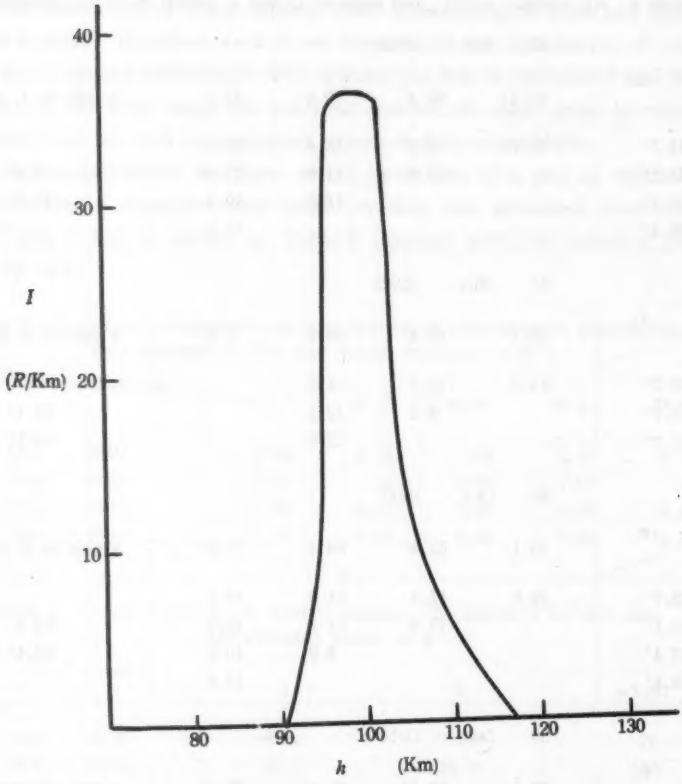

Fig. 3. Height of emitting layer reported by Heppner and Meredith (rocket observation).

measurement by our method will be impossible. Fortunately, such fluctuations were not experienced during the IGY and the ICC.

4. Supplementary Note

By the use of an expression other than δ_s employed in the preceding sections, the height of the layer can also be found.

At each of the two stations, the photometer, description of which is given in Section 3, is set faced to each other, and six altitude observations on the intensity of glow are made (Fig. 4).

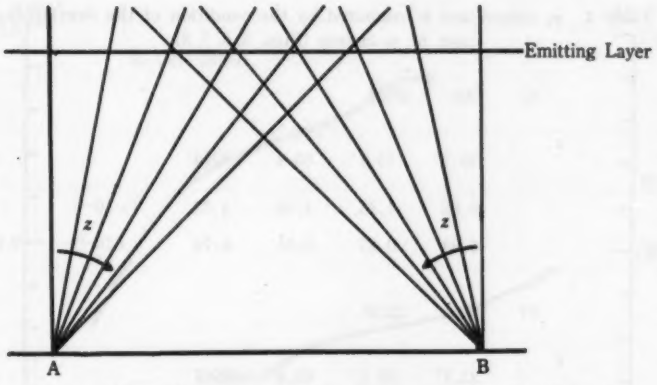

Fig. 4. Schematic diagram of the measurement by directing the telescope to six altitudes.

The expression proposed above is

$$\sigma_z=\frac{\sqrt{\sum\{R(z,t)-\overline{R(z)}\}^2/N}}{\overline{R(z)}}=\sqrt{\sum\{R'(z,t)-1\}^2/N}.$$

The variations of σ_z against z recorded at the two stations are plotted and compared. If two stations observe the emitting layer at the same time, these σ_z curves must partly lie one upon another. From this overlapping part, z_1 and z_2 that can be used in (2.4) can be obtained and the height of the layer can be calculated. The results are shown in Table 4.

Acknowledgement

The writer expresses his sincere thanks to Prof. T. Suga and Prof. K. Yoshihara of Nagoya University for their valuable advice and encouragement, to Prof. M. Huruhata of Tokyo Astronomical Observatory for his guidance and to Mr. T. Ichikawa for help in field work and compiling of data.

Table 4. σ_z values and h computed by the condition of the overlapping part of σ_z curves (Figs. 5, 6, 7, 8).

57 Oct. 23/24

z / Station	33.7°	53.1°	63.4°	69.4°		h(km)
Gifu	0.85	1.15	1.24	1.33	($\times 10^{-1}$)	89
Sendai	0.94	0.85	0.81	0.74	($\times 10^{-1}$)	

57 Nov. 22/23

z / Station	33.7°	53.1°	63.4°	69.4°		h(km)
Gifu	1.60	1.51	1.46	1.77	($\times 10^{-1}$)	109
Sendai	1.50	1.36	1.31	1.21	($\times 10^{-1}$)	

58 Oct. 16/17

z / Station	33.7°	53.1°	63.4°	69.4°	75.0°		h(km)
Gifu	1.89	1.91	1.76	1.85	1.76	($\times 10^{-1}$)	81
Sendai	1.43	1.58	1.67	1.67	—	($\times 10^{-1}$)	

58 Dec. 13/14

z / Station	33.7°	53.1°	63.4°	69.4°	75.0°		h(km)
Gifu	3.30	3.19	2.86	3.37	3.23	($\times 10^{-1}$)	89
Sendai	2.59	2.71	2.47	2.29	2.66	($\times 10^{-1}$)	

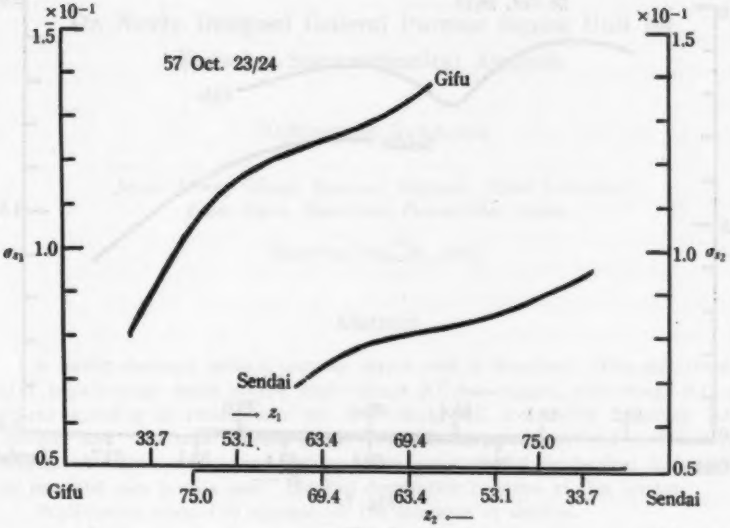
×10⁻¹
1.5
57 Oct. 23/24
Gifu
×10⁻¹
1.5
σs1 1.0
1.0 σs2
Sendai
→ z1
33.7
53.1
63.4
69.4
75.0
0.5
0.5
Gifu
75.0
69.4
63.4
53.1
33.7
Sendai
z2 ←

Fig. 5.

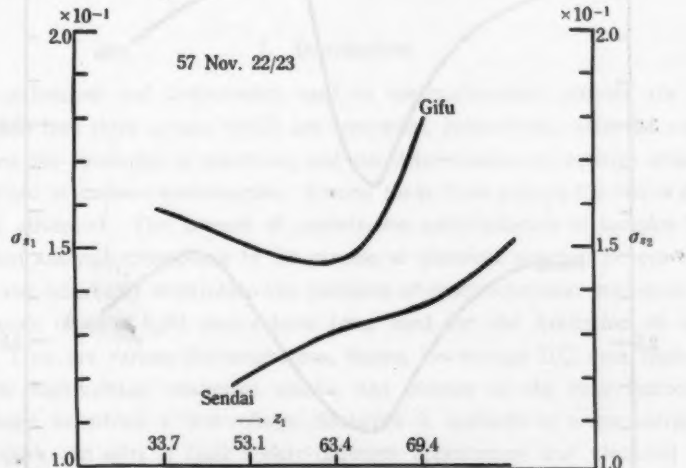
×10⁻¹
2.0
57 Nov. 22/23
×10⁻¹
2.0
Gifu
σs1 1.5
1.5 σs2
Sendai
→ z1
33.7
53.1
63.4
69.4
1.0
1.0
Gifu
69.4
63.4
53.1
33.7
Sendai
z2 ←

Fig. 6.

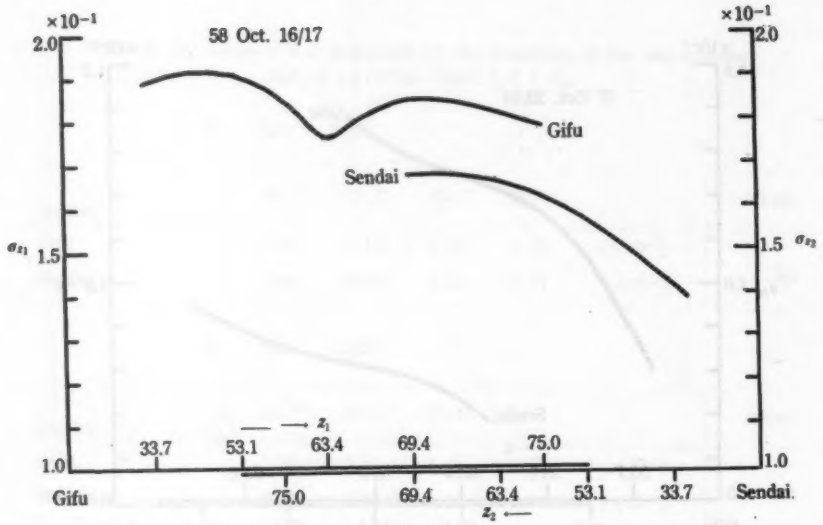
×10⁻¹
2.0
58 Oct. 16/17
Gifu
Sendai
σ_{z1}
1.5
1.0
z_1
33.7
53.1
63.4
69.4
75.0
Gifu
z_2
Sendai
σ_{z2}

Fig. 7.

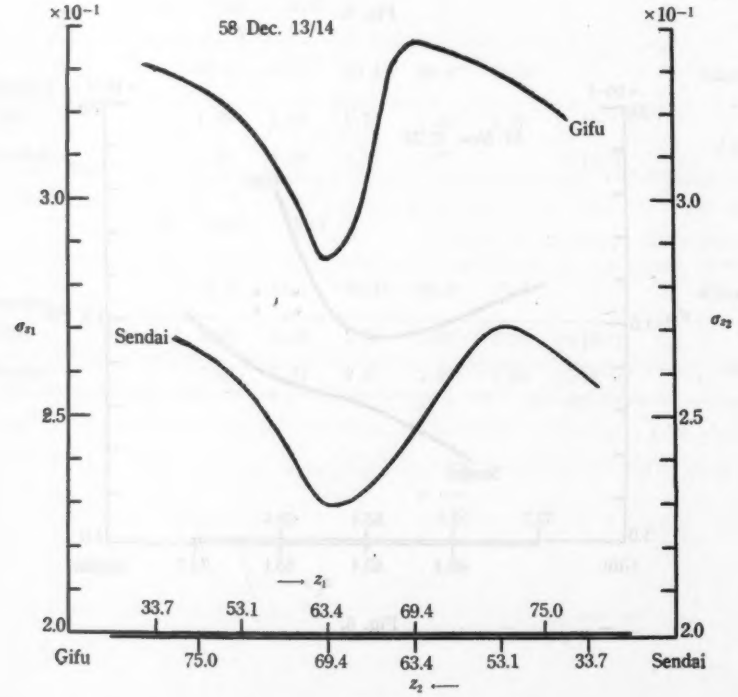
×10⁻¹
58 Dec. 13/14
Gifu
Sendai
3.0
2.5
2.0
σ_{z1}
σ_{z2}
z_1
33.7
53.1
63.4
69.4
75.0
Gifu
z_2
Sendai

Fig. 8.

SCIENCE OF LIGHT VOLUME 10, NUMBER 2, 1961

On Newly Designed General Purpose Source Unit for Emission Spectrochemical Analysis

Tokunosuke NAKAJIMA

Japan Atomic Energy Research Institute, Tokai Laboratory
Tokai-Mura, Naka-Gun, Ibaraki-Ken, Japan

(Received Feb. 24, 1961)

Abstract

A newly designed general purpose source unit is described. The unit consists of a high-voltage spark source, high-voltage A.C. arc source, low-voltage A.C. arc source including an intermittent arc, low-voltage D.C. arc source including intermittent and "uni-arcs", multi-source type discharge source and a Walsh-type source. A fully synchronized igniting pulse generator of mechanical design plays an essential role in this unit. Detailed description is given of this ignitor.

Push-button control is adopted for the selection of sources.

Considerations on discharge conditions are also described. Performance of sources of various types is demonstrated by voltage and/or current oscillograms, photographs of parts are shown.

1. Introduction

The techniques and instruments used in spectrochemical analysis are usually divided each into three groups which are concerned, respectively, with the excitation of samples, the resolution of spectrum, and the determination of relative intensity of light emitted at various wavelengths. Among these three groups, the first is probably the least advanced. The process of vaporization and excitation of samples in spectrochemical analysis corresponds to the process of chemical reaction in wet chemical analysis and inherently determines the precision of spectrochemical procedure.

Six main types of light source have been used for the excitation of emission spectra. They are various discharge tubes, flames, low-voltage D.C. arcs, high-voltage A.C. arcs, high-voltage condensed sparks, and sources of the type introduced by Pfeilsticker[1] in which a low-voltage discharge is initiated by a low-energy, high-voltage spark. In spite of their widely different appearances and electrical characteristics, all of them are specialized forms of gas discharge. Therefore, internal mechanisms for excitation are essentially the same.

1) K. Pfeilsticker; Zeitsch. Electrochem., **43** (1937) 719.

For example, the discharge produced by so-called spark circuits is in fact an arc as clearly stated by Kaiser[2], the spark serving only to initiate the discharge, and the light emission of the spark is negligible from the view point of spectrochemical analysis.

Recently, Mandel'shtam[3] reported that the intrinsic difference between sparks and arcs is the difference in current densities in their discharge plasmas. This difference is caused by the difference in respective diameters of discharge channels. The conditions of external circuits, spark circuit for example, determine how much energy can be released into such a thin spark channel within a limited time. For instance, if the energy stored in a capacitor is dissipated within such a short time as 10^{-7}~10^{-6} sec, spark channel will be thin. But soon the spark channel begins to broaden and becomes a plasma which is identical with that of the arc plasma. The evaporation of electrode material, which is a more basal problem in spectrochemical analysis, occurs only after such processes.

The energy of plasma may transforms into the energy of evaporation, detailed mechanism of this transformation is not known. Nevertheless, a spark is none other than an arc in a transient state, and proper control of the arc is the crucial problem in quantitative spectrography.

It is indeed the preoccupation with this problem which is the distinction between spectrography for chemical analysis and what is usually understood by spectroscopy. According to Sherman[4], the problem of control of the arc may be divided into two parts, the first of which is to devise some source of excitation that would generate and maintain a precisely reproducible radiating arc (of the same temperature), and the second is that the distribution of elements present in the arc should be simply correlated with the concentration or distribution of the elements in the electrode. There have been no excitation sources that fulfill the above requirements. So, many types of the sources or circuits have been devised and it has been believed that those devices can contribute to the improvement on precision of analytical results. In fact the improvement was concerned only with electrical characteristics of sources or circuits.

In other words, it has long been assumed that a circuit, if stable from usual electrical view-point, will give rise to a reproducible radiating arc. This condition appears physically necessary but it is not known whether it is sufficient. The chances are that it is not.

---

2) H. Kaiser and A. Wallraff; Ann. Phys., **34** (1939) 297.

3) S. Mandel'shtam; Spectrochim. Acta, (1959) 255.

4) J. Sherman; "Physical Methods in Chemical Analysis" page 278 Edited by W.G. Berl, Academic Press Inc. Publishers, New York (1950).

The trend of modern development appears to be in generating periodical bursts of radiating gas in small amounts allowing the arc to be extinguished and the vapors to be removed from the reactive zone between successive bursts.

It is easily seen that the circuits of Pfeilsticker's type are suitable for those purposes. But future research should be concentrated on studying the evaporation and excitation process and also on clarifying the correlation between those processes and the electrical conditions.

The author's opinion is as follows. The study on evaporation and excitation process in spectrochemical analysis should be defined as the science concerning the mutual interaction between electrical discharge and electrode material. Therefore, what is expected from excitation sources is not to get a source that would give the best analytical results but to devise a source that would give as many types of discharge as possible with discharge characteristics that must be well known electrically at least and also physically if possible.

In addition, it is implicitly assumed that the source parameters in the circuit were so selected that the generated discharge could develope favourably the emission spectrum from 2200 Å to 5000 Å which includes the almost persistent lines of the elements. From the considerations mentioned above, the sources which are described in the next section, are assembled in one unit. Those sources are selected in order to represent each of the main types of source which have been used to date except flames and discharge tubes. The circuit systems are selected mainly from the experience of the author in analyzing the results on all types of sources of various design made for trial. At the same time it is intended to obtain as many sources as possible if simple rearrangement of circuit components allows to turn out other design of source. Needless to say, the source unit thus obtained allows one to select versatile exciting conditions, which are suitable respectively for widely different types or natures of analytical samples. This means that the unit may conveniently be used for practical analysis also.

2. Description of the Sources

1. Spark source

Wiring diagram of spark source is shown in Fig. 1. Raiskij introduced this scheme into the practical spectroscopy which was already described by the author[5]. The author had also reported that this simple tandem spark exhibited several features: unlike the case of the Feussner spark, it does not include any of the rotating components; especially, the influence of line-voltage fluctuation does not affect the charging

5) T. Nakajima and S. Shibuya; Bunko Kenkyu, No. 8, (1954) 14. (In Japanese)

voltage of capacitor and thus practically gave very good precision in analysis. "Raiskij spark" is being widely used as a standard source for spectrographic analysis of iron and steel in Japan. The improvements that have been made this time on the source is as follows.

1) Capacitance of the discharge capacitor can be increased from 0.003 μF to 0.016 μF in 6 steps.

2) Corresponding to the changes in capacitance (1-C-4, 5, 6, 7 in Fig. 1), resistance of ohmic resistor 1-R-1 is automatically adjusted to a predetermined value at which a slightly over-damped condition of the charging cycle is fulfilled.

3) The number of discharges per half cycle can be increased as many as one wishes if only the charging circuit permits. Over twelve discharges per half cycle may be possible. Blowing of nonturbulent air stream across the control gap is necessary to attain this maximum number of breaks.

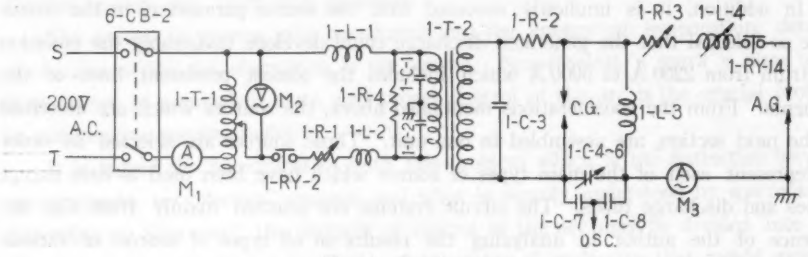

Fig. 1. Spark source.

1-R-1:	primary resistor, 9~30Ω variable, max. 30 amp.
1-R-2:	secondary resistor, 2.5 KΩ, 200 W.
1-R-3:	discharge resistor, 0~3Ω, variable, wire wound.
1-R-4:	surge absorbing resistor, 10 KΩ, 20 W.
1-C-1, 2:	surge absorbing condensers, 0.5 μF, 1000 V.
1-C-3:	mica condenser, 500 $\mu\mu$F, 40 KV.
1-C-4~7:	main oscillating condensers, 2×0.003 μF, 2×0.005 μF, 40 KV mica condenser.
1-C-8:	condenser, 4 μF, 1000 V.
1-L-1, 2:	inductance coils.
1-L-3:	inductance coil, 1600 μH.
1-L-4:	inductance coil, max. 1000 μH, 4-tapped.
1-T-1:	variable transformer, 220/0~260 V, 3 KVA continuous.
1-T-2:	main transformer, 220/22,000 V, 7.5 KVA, oil insulation.
M_1:	ammeter, M_2=voltmeter, M_3=R.F. meter, 15 amp.
6-CB-2:	instantaneous type circuit breaker, 30 amp.
1-Ry-2:	magnet switch, DPST, 50 amp.
1-Ry-2:	vacuum switch.
C.G.:	control gap.
A.G.:	analytical gap.

4) Series inductance 1-L-4 in the discharge circuit can be varied from residual to 1000 μH in 4 steps.

5) Precise adjustment of gap length of the control gap can be made from outside on optical projection of the gap.

6) A RF-current meter is inserted into the discharge circuit.

7) Coils are sealed with special plastics to reduce "corona losses".

2. High-voltage A.C. arc source[6][7]

Wiring daigram of high-voltage A.C. arc source is shown in Fig. 2. In the circuit of high-voltage A.C. arc source, ohmic resistance or variable inductance is generally used as a series impedor.

The author has favored the ohmic resistance because a resistance-type source can be easily modified to a "hot arc" generator[8].

But the drawback of the ohmic resistor is that the input energy is bound to be dissipated as Joule heat so that much heat is generated in the instrument causing an undesirable temperature rise. Need of a large space for the apparatus is therefore unavoidable. Necessity of packing as many parts as possible in a limited space forced the author to adopt a variable reactor of the moving iron core type as an impedor. An over-all view of the reactor is shown in Fig. 3.

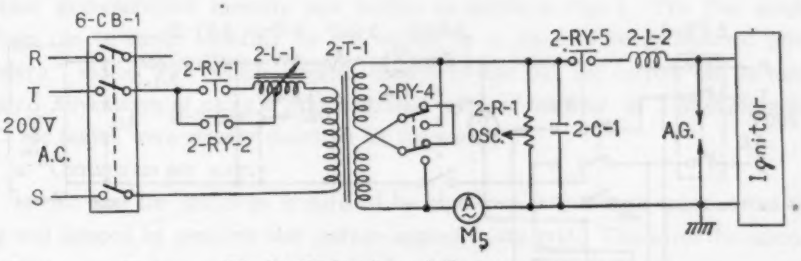

Fig. 2. High-voltage A.C. arc source.

2-R-1:	carbon resistor, 10 MΩ, 10 W.	6-CB-1:	main switch, circuit breaker 60 amp.
2-C-1:	filter condenser, 0.1 μF, 10 KV.	M_5:	ammeter, 5 amp.
2-L-1:	moving iron core type reactor.	2-Ry-1, 2:	magnet switches, DPDT, 50 amp.
2-L-2:	inductance coil, air core, 800 μH.	2-Ry-4:	long arm relay.
2-T-1:	main transformer, 220/2400×2 V, 12 KVA.	2-Ry-5:	vacuum switch.

6) O. S. Duffendack and R. A. Wolfe; Proceedings, 5th Summer Conf. on Spectroscopy and its Applications, John Wiley & Sons, New York, N. Y. (1938).

7) T. Nakajima, T. Mitsuhashi and Y. Shiraishi; J. Mechanical Lab, A. I. S. T. Japan 2, (1951) 197.

8) T. Nakajima and Y. Shiraishi; Bunko Kenkyu. No. 6 (1953) 20

Fig. 3. Moving iron core reactor for high-voltage A.C. arc source.

The central iron core is pulled in or out with the aid of a pulley and a driving motor.

3. Low-voltage A.C. arc source

A schematic diagram of low-voltage A.C. arc source is shown in Fig. 4. In the circuit the discharge can not be self-sustained if the arc current is within a certain range; the discharges quench themselves at the end of every half cycle. In order to maintain the arc discharge, a high-voltage low-energy spark must be introduced across the analytical gap at every half cycle. In other words, main discharges can be controlled by igniting discharges. This type of source was first introduced by Pfeilsticker[1] and is regarded as the prototype of the mordern "Triggered source". Voltage and current wave forms of the discharge and period of the discharge can be widely controlled by proper settings of repetition rate or electrical phase of the igniting pulse against power line wave. Thus the igniting pulse

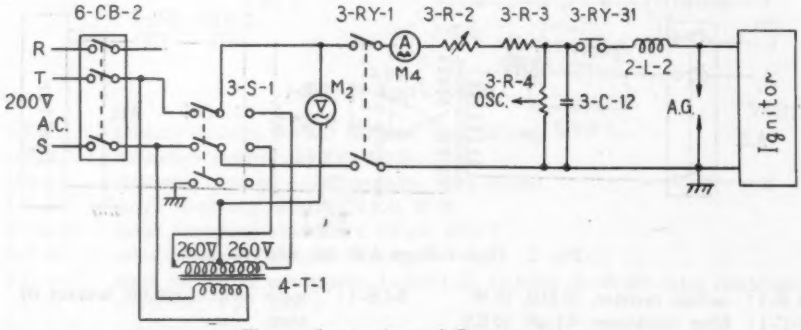

Fig. 4. Low-voltage A.C. arc source.

3-R-2: ohmic resistor, max. 290 Ω, max. 30 amp.
3-R-3: ohmic resistor, 10 Ω fixed, max. 30 amp.
3-R-4: voltage dividing registor, 100 KΩ, 5 W.
3-C-12: filter condenser, 0.1 μF, 1000 V.
4-T-1: Refer to Fig. 5.
3-S-1: transfer switch, Refer to Fig. 20 (a).
3-Ry-1: magnet relay, Tateishi AV-type, coil; 24 V 80 ma, contacts; 45 amp. (not a breaking capacity), DPST.
3-Ry-31: vacuum switch.
M_4: R.F. meter, dual ranges 5/15 amp.

generator plays a main role in this type of sources. Detailed description of the igniting pulse generator will be given later. A.C. service of 200 V is simply used as the power source. In this case the variable series resistor is the only parameter. This design is very simple but the following should be considered.

If the line voltage of power circuit becomes lower than that of the arc-sustaining voltage, the presence of igniting pulse across the gap does not matter at all. This means that the igniting pulse must be present in the central region of sinusoidal wave form of power supply. To assure re-ignition of the main discharge, this region must be limited to a narrow central portion. (Refer to Fig. 23)

It is expected that the region, in which the main discharge can be triggered by igniting pulse, is widened if the line voltage is elevated. For this elevation, 200 volt line is switched over by switch 3-S-1, Fig. 4, to 520 volt (rms) line of transformer 4-T-1, Fig. 4.

Actually a transformer in D.C. arc circuit is utilized for this purpose. In this case, arc current must be limited to under 10 amp. on account of limited current capacity of the transformer leg.

4. Low-voltage D.C. arc source

The basic circuit of low-voltage D.C. arc source is a rectifier circuit using a 6-phase grid-controlled mercury pool rectifier as shown in Fig. 5. The D.C. output voltage can be varied smoothly by the action or a phase shifting network using "Selsyn" motor with which stepless control of the D.C. arc current can be made easily. Advantages of using a grid controlled mercury rectifier as a spectrographic D.C. arc source were already described by the author[9].

a. Continuous arc source

In this case the discharge is initiated by high-frequency trigger spark across the gap and stopped by negative bias voltage applied to the grid. This saves the expence of using a heavy-duty magnetic switch. In order to reduce the ripple voltage, series choke (4-L-2) and parallel capacitor (3-C-8) are inserted. From the correlation found between the capacitance value of 3-C-8 and the ease in arc firing, 50 μF was selected experimentally as the optimal value of capacitance.

b. Intermittent D.C. arc source

Interruptions of the main discharge can be achieved by on-off action of the grid. In this case the filtering network consisting of 4-L-2 and 3-C-8 must be removed from the circuit. The on-off pulse applied to the control grid is generated from a cam-shaft interrupter (described later) and is synchronized to the high frequency igniting pulse across the analytical gap.

9) T. Nakajima and S. Saegusa; Bunko Kenkyu, **3**, (1952) 8.

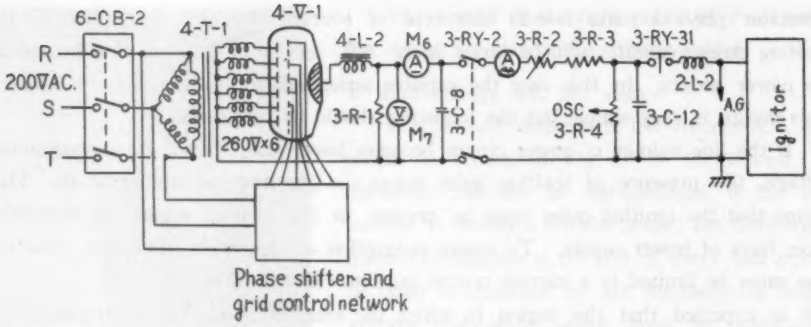

Fig. 5. Low-voltage D.C. arc source.

3-R-1: wire resistor, 300 Ω, 1 KW.
3-C-8: condenser, 50 μF, 1000 V.
4-L-2: choke, 20 mH, max. 30 amp.
4-V-1: 6-phases, grid controlled mercury pool rectifier, Toshiba M3GM-30-E_3.
4-T-1: main transformer, Δ-YY connection, 220 V/280 V.
3-Ry-2: magnet relay, same as 3-Ry-1.
M_6: d.c. ammeter, 30 amp.
M_7: d.c. voltmeter, 400 V.

5. "Uni-directional arc" source

A schematic diagram is shown in Fig. 6. Actually, 4-V-1 is one of the arms of the 6-phase mercury rectifier tube and the other five arms are in cut-off state by negative bias applied to their respective grids. Typical voltage wave forms obtained from this type of source are shown in Fig. 25. Comparison of this wave-form with that obtained from the low-voltage A.C. arc source, provided the igniting pulse is supplied at a rate of 50 pulses per second, (Fig. 23) does not seem to give any essential difference between these two sources. The only difference is that the former extinguishes the arc plasma in rectifier tube and the latter does the same in open air. However, some investigators[10][11] reported that this uni-directionnl arc source had given good analytical results. Thus it was decided to build this source for the present unit, because only minimum modifications of D.C. arc circuitry are required.

"Jaco Varisource" also uses this type of source. In Varisource, the discharge is ignited by a high-voltage air-jet type spark instead of igniting pulse which is used by the author.

If the spark discharge in arc plasma has some significant influence on spectral excitation, results obtained from these two sources will be different. Further com-

10) A. J. Mitteldorf; Anal. Chem. **29** (1957) 17A.
11) R. F. Farrell, G. J. Harter and R. M. Jacobs; Anal. Chem. **31** (1959) 1551.

parative experiments on this type of source are desirable.

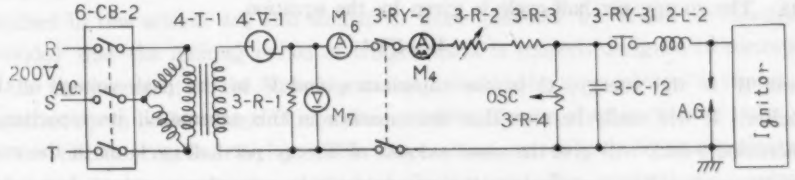

Fig. 6. Uni-directional arc source.

3-R-1: Ref. to Fig. 5. 2-L-2: Ref. to Fig. 2.
3-R-2, 4: Ref. to Fig. 4. 4-T-1: Ref. to Fig. 5.
3-C-12: Ref. to Fig. 4. 4-V-1: Ref. to Fig. 5.

6 Multi-source type discharge source

A block diagram of Multi-source unit developed by Hasler and Dietert[12] is shown in Fig. 7. The mode of operation for the unit will readily be understood from this block diagram. In one half-cycle of the supply main, capacitor C is charged to a voltage of about 100 volts, while in the next half-cycle the high-frequency generator passes a spark across the analytical gap, resulting in the discharge of C through inductance L, resistance R and the analytical gap. One of the unique features of this scheme is that the discharging and charging of C go on independently, eliminating possible mutual interaction between these two processes, each process becoming separately controllable. Another feature is its versatility; many combinations of C, R, and L are possible. The source provides a variety of discharge conditions as shown in Fig. 26.

Similar circuits may be devised by utilizing one phase of the 6-phase mercury

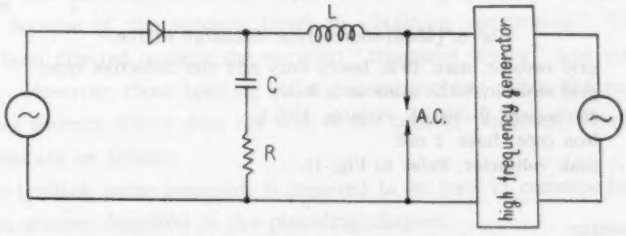

Fig. 7. Hasler-Dietert multi-source and B.N.F. general purpose source unit. Diagram illustrating mode of operation of the units.

12) M. F. Hasler and H. W Dietert; J. O. S. A. **33** (1943) 218.

pool rectifier. The maximum inverse withstand voltage of the rectifier tube being considered, the maximum charging voltage of capacitor C is limited to about 300 volts. The energy per half-cycle is given by the equation

$$W=CV^2$$

where W is the energy, C is the capacitance and V is the peak voltage of the capacitor. It will easily be seen that the capacitor in this scheme, if its capacitance is increased 9-fold, will give the same amount of energy per half-cycle as in the case of multi-source. Yet, considering that any increase in capacitance means inevitable increase in time constant of discharge circuit and also that the discharge process must be completed in one half-cycle, we see the advantage of multi-source over the above scheme. However, since mere insertion of a suitable capacitor into D.C. arc source circuit turns the above scheme into multi-source type, it was finally decided to increase the capacitance, and a capacitor bank of 500 μF was installed. The capacitor bank is arranged after the principle of weights of chemical balance: it comprises capacitors of 1, 2, 2, 5, 10, 10, 20, 50, 100, 100 and 200 μF so that by parallel switching any desired capacitance between 0 and 500 μF in 1 μF steps can be obtained. Rectifier tubes with thermoionic emission type cathode, which are generally used in this type of source, are very weak to excessive currents. The mercury pool rectifier in the author's scheme is excellent in this point and sufficiently withstands a large rush current required for charging a large capacitance.

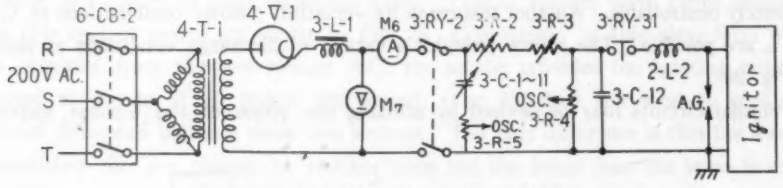

Fig. 8.[1] Multi-source type discharge source.

3-R-3: grid resistor, max. 10 Ω, heavy duty and non inductive type.
3-R-5: grid resistor, 0.2 Ω, same as 3-R-3.
3-C-1, 11: condensers, 0~500 μF variable, 1000 V.
3-L-1: iron core choke, 2 mH.
M_7: peak voltmeter, Refer to Fig. 17.

7. Walsh source

By insertion of a variable resistance into a charging circuit as shown in Fig. 9, a source similar to that described by Walsh[13] can be obtained. The resistance

13) A. Walsh; Met. Ind. **68** (1946) 243.

described in Fig. 8 is divided into two parts, one part of which is transferred to the charging side of main C. (3-C-1-11) (Refer to Fig. 9) The discharge wave forms obtained in this scheme are also similar to those obtained by Walsh or Sinclair[14], provided that the igniting period of trigger spark is properly assigned to correspond to the time constant of the charging circuit. Should the time required to charge the capacitor up to peak voltage of the main exceeds 10 msec. (half-cycle), the pulse rate of the initiator needs reducing. This can be done conveniently by an electronically controlled igniting pulse generator (described later). For mechanically controlled igniting pulse generator, a special cam must be provided.

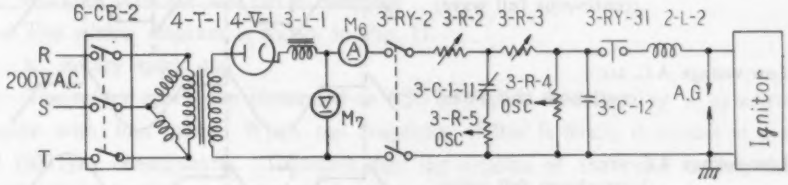

Fig. 9. Walsh' source.

3-R-2, 4: Ref. to Fig. 4. 3-L-2: Ref. to Fig. 2.
3-R-3, 5: Ref. to Fig. 8. 4-T-1: Ref. to Fig. 5.
3-C-1, 11: Ref. to Fig. 8. 4-V-1: Ref. to Fig. 5.
3-C-12: Ref. to Fig. 4. M_7: Ref. to Fig. 17.
3-L-1: Ref. to Fig. 8.

3. Fully Synchronized Igniting Pulse Generator of Mechanical Scheme

1. Design considerations on igniting pulse generator

In preceding chapters it has been shown that the igniting pulse plays an essential role in this instrument. Many types of igniting pulse generator have been devised[14][15] because of the modern trend in obtaining spectroscopic light sources which has been directed towards the so-called "triggered source" first introduced by Preilsticker. However, those igniting pulse generators have a function only sufficient for particular sources, which does not suit to the present purposes. Required design considerations are as follows.

a. The igniting pulse generator is required to be used in common for triggering the different sources described in the preceding chapter.

b. The phase relation between the trigger pulse and the power line is required to vary freely and continuously from 0 to 360 electrical degrees.

14) D. S. Sinclair; J. O. S. A. 38 (1948) 547.
15) H. Buckert; Spectrochim. Acta. 4 (1952) 525.

c. The output energy of the igniting pulse should remain constant, independent of the phase rotation.

d. The intermittent period should synchronize with the main power line.

e. Setting of correct phase of pulse for every source should be automatic.

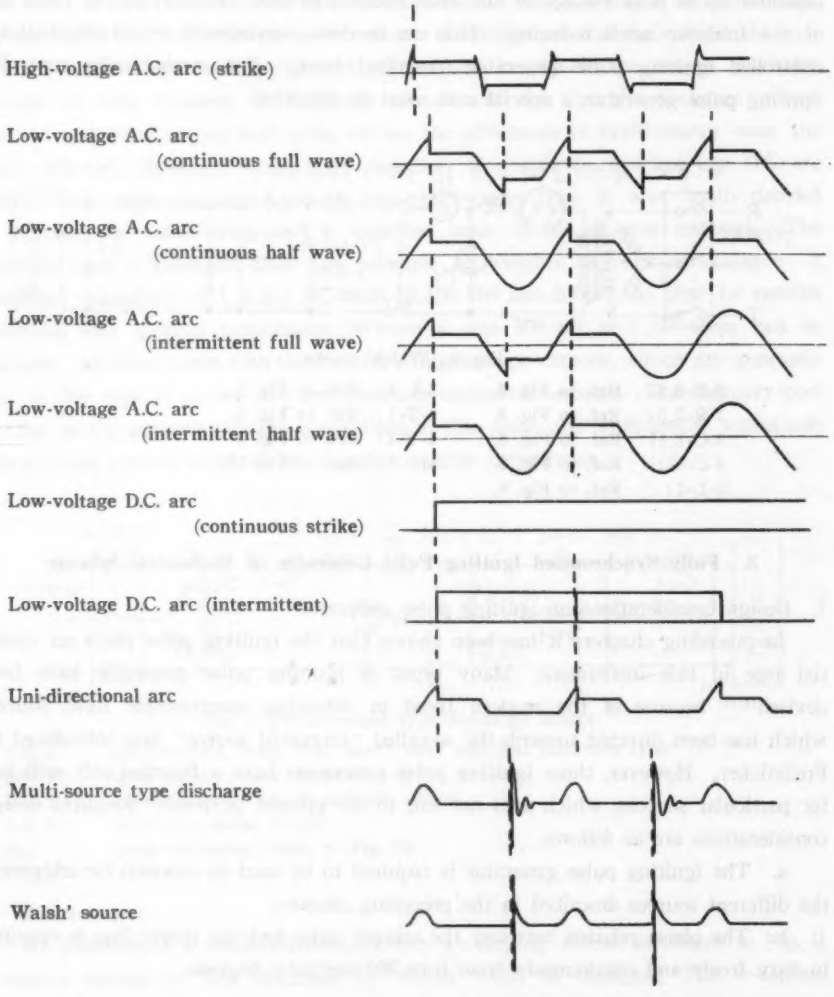

Fig. 10. Phase relation between trigger pulse and the sources; dashed lines show the positions of triger pulses.

2. Phase relations between trigger pulse and various main discharges

Fig. 10 summarizes the phase relations between trigger pulse and the sources described in the preceding chapter. It is easily seen that the trigger pulse is needed only for the initiation of discharges in high voltage A.C. and low voltage D.C. arcs. The need is fulfilled by cutting off the holding circuit of 5-Ry-1 in Fig. 11 whereby the igniting pulses are generated only when the "start" button is depressed. Accordingly, D.C. mains must be interrupted in order to interrupt D.C. arcs. It is also seen from Fig. 10 that pulse rates of 50 per second and 100 per second are both required.

3. Working principle and circuit diagram

The wiring diagram is shown in Fig. 11.

a. Rotary spark gap

The rotary spark gap illustrated as RSG in Fig. 11 is driven by a synchronous motor with four poles. When the frequency of line is 50 c/s, it rotates at a speed of 1500 rpm, consequently. Therefore, half the rotation of the rotor corresponds to one cycle of the power line. Since one trigger spark must be generated per cycle at least, the rotating disc, which is fixed directly on the end of the rotor's shaft, must have two poles, which will be a part of the spark gap. These poles are located at 180° angles with each other on the rotating disc, which means that there are two synchronizing positions each of which includes two identical positions spacely. These two positions have the same probabilities and hence can change over with each other at every starting of the motor.

In order to avert the above phenomenon and to obtain a trigger spark at the identical phase angle, some devices are provided in this network.

First, a phase detecting commutator is fixed on the rotor shaft. Fig. 11 shows the commutator in a conductive phase and, hence relay (5-Ry-7 in Fig. 11) is acting and thus holding vacuum switch (5-Ry-9). Therefore capacitor 5-C-1 discharges through stator A. In the other synchronizing position of the commutator, the current of 5-Ry-7 is being cut and in this case capacitor 5-C-1 discharges through stator B. After all, the phase of the igniting spark is held constant against the phase of the power line. Needless to say, stators A and B are located at right angle to each other 180 degrees electrically. Since the current through 5-Ry-7 is pulsating, a relay having a shading coil is chosen so that chatterings of its contacts may not occur. 5-V-1 and 5-V-2 are kenetron tubes, therefore, capacitor 5-C-1 is charged by direct current. The rotating gap discharges the capacitor only after capacitor 5-C-1 has been charged. In this way, the charged-up voltage of capacitor 5-C-1 remains the same over large electric angles. Consequently, output energy of the

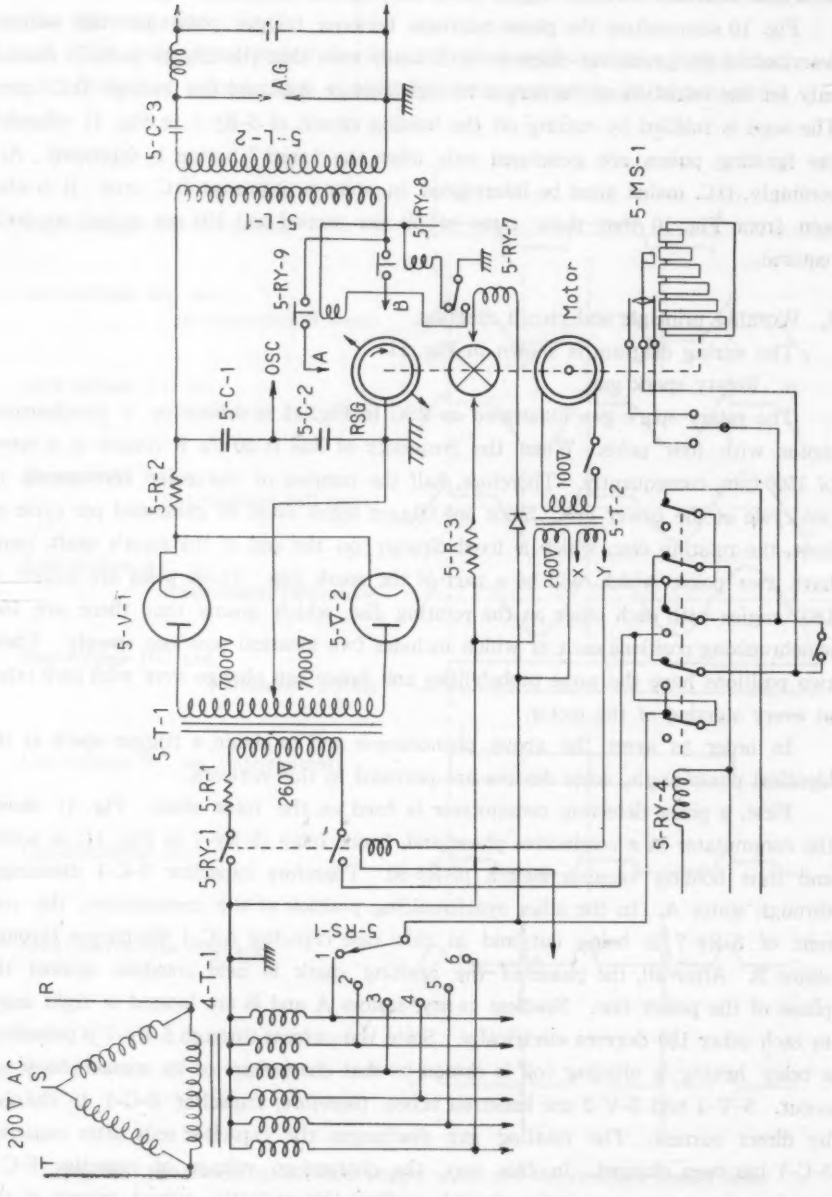
5-C-3
A.G
5-L-2
5-L-1
5-RY-8
5-RY-9
5-RY-7
5-MS-1
Motor
B
A
OSC
5-C-1
5-C-2
RSG
5-R-2
5-R-3
100V
260V
X
Y
5-T-2
5-V-1
5-V-2
7000V
7000V
5-T-1
260V
5-R-1
5-RY-1
5-RY-4
5-RS-1
1
2
3
4
5
6
4-T-1
R
S
T
200V AC

igniting pulse can be held constant. The rotation of the stator on the concentric circle of the rotor permits the change in ignition phase of the trigger spark without changing the output energy. Because the phase relations among the parts of this network are complicated as mentioned above, voltage waves of the parts are as shown schematically in Fig. 12. Actually, the adjustment can be easily made with the aid of an oscilloscope. In addition, the power line for the spark generator and synchronous motor is fed from one of the secondary windings of a delta-double-star-connection power transformer for the 6-phase mercury rectifier tube mentioned before, and the power line rotates sequentially because electric phase of the each secondary windings rotates at intervals of 60 degrees. This means that one can shift the phase of the igniting spark against the main discharge. Since the stator can be rotated over 90 degrees, only the changing of the power line from one winding to the next suffices for the shifting of igniting pulse over all electric degrees. A SPDT* switch is provided for this purpose. It must be noted that a considerably high surge is expected since the network includes such inductive loads as a motor. Close attention was paid to the choice of this switch.

b. Interrupter with cam-shaft controller

A cam-shaft controller is installed on the shaft of a reduction gear which is coupled directly to the shaft of a synchronous motor. Since the reduction ratio of 1/25 is preferred, rotation of the cam-shaft is adjusted to one revolution per second. A micro-switch actuated by the cam controls on and-off of circuits. Impulse ratios of the cam-shaft are selected as shown in Table 1 on the consideration of one revolu-

* Single pole double throw.

Fig. 11. Fully synchronized igniting pulse generator.

5-R-1:	enamelled resistor, 10 Ω, 200 W.
5-R-2:	enamelled resistor, 20 KΩ, 10 W.
5-R-3:	wire resistor, 4 KΩ, 10 W.
5-C-1:	oscillating capacitor, 0.002 μF, 20 KV.
5-C-2:	condenser, 0.5 μF, 1000 V.
5-C-3:	tuning mica condenser, 500 μμF, 40 KV.
5-L-1:	primary of Tesla coil, 12 μH.
5-L-2:	secondary of Tesla coil, 110 μH.
5-T-1:	leakage transformer, 260/7000×2 V, 200 VA.
5-T-2:	transformer, 260/100 V, 50 VA.
5-V-1, 2:	Kenetron tubes, 1-K-22.
5-Ry-1:	relay, coil; 24 V, 35 ma, contacts; 5 amp. DPDT.
5-Ry-4:	relay, coil; 24 V, 35 ma, contacts; 5 amp. 6PDT.
5-Ry-7:	relay, coil; 100 V ac, 35 ma; DPDT.
5-Ry-8, 9:	vacuum switches.
5-MS-1:	micro switch, SPDT.

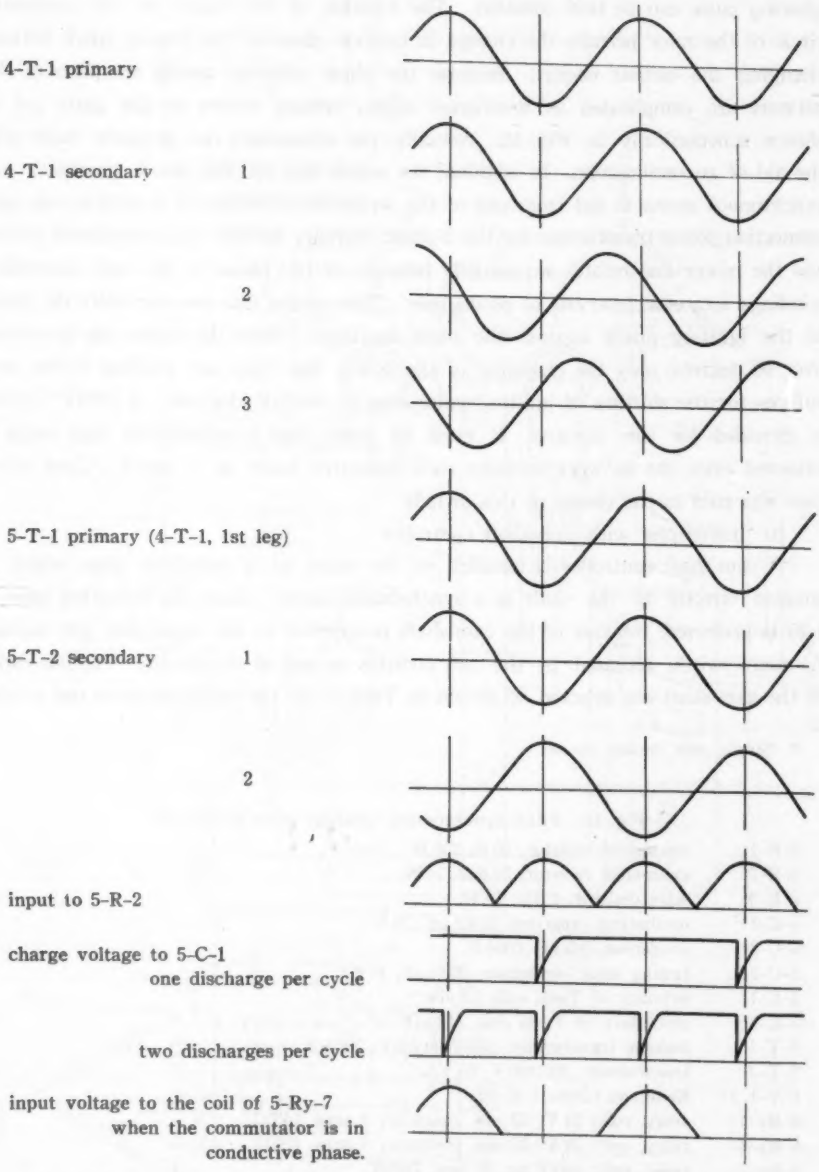

Fig. 12. Phase relation in the igniting pulse generator illustrated in voltage wave form.

tion corresponding to 50 cycles. The combination of the impulse ratios shown in Table 1 is deduced from practical experience. Any other impulse ratios can also be obtained at will by exchanging the cam-shaft. The rate of interruption per revolution is fixed purposely for simplicity of the apparatus and for reproducibility of experimental condition. The micro-switch is of the single pole and double throw type, and hence reversed impulse ratios can be easily obtained by adding a transfer switch, by which means doubled cases of the impulse ratio as shown in Table 1 are obtained. (28 cases) 5-Ry-4 in Fig. 11 is used to transfer the micro-switch from the circuit of A.C. intermittent arc to that of D.C. intermittent arc For A.C. arc, the micro-switch is inserted in series in the primary of transformer 5-T-1. In the case of D.C. arc, this micro-switch controls both the grid relay of the 6-phase mercury rectifier and the igniting pulse generator.

Table 1. Combination of impulse ratios furnished by the cam-shaft.

Total period	1 sec.		2 sec.	
cases	discharging cycle	stopping cycle	discharging cycle	stopping cycle
1	2(48)	48(2)	1(24)	24(1)
2	4(46)	46(4)	2(23)	23(2)
3	6(44)	44(6)	3(22)	22(3)
4	10(40)	40(10)	5(20)	20(5)
5	12(38)	38(12)	6(19)	19(6)
6	16(34)	34(16)	8(17)	17(8)
7	24(26)	26(24)	12(13)	13(12)

Figures in parentheses show the cases where the micro-switch is reversed.

c. Electronically Controlled Igniting Pulse Generator

An electronically controlled igniting pulse generator utilizing a Dekatron counting tube and incorporating a impulse generator using Cockcraft-Walton circuit is installed also. However, this generator is often removed from the unit and used separately as an independent source. Full description of the generator will be made elsewhere in the near future.

4. Automatic Operation and Measure for Safety

1. Control circuit

Selection of sources and their several source parameters is performed by relay networks incorporated in the unit. The power voltage of the relay network is fixed at 24 V D.C. in order to utilize telephone relays. A selenium rectifier of D.C. 24 volt and maximum 10 amp. output is used as the power source for the control circuit.

Wiring of the relay network is too complicated to be illustrated on diagram. Brief comments will be given in the following section to explain its working action.

a. Source selector

Fig. 13 shows the source selector. Each of the push-buttons has eight independent contacts. If the required number of contacts exceeds eight, a multiple contact relay is added. Use of silicon or germanium diodes is effective to simplify the network by utilizing their valve actions.

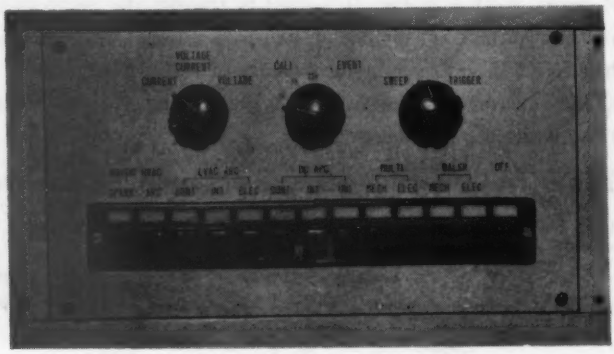

Fig. 13. Source Selector Switch.

b. Timer circuit

For automatic control of pre-discharge time and exposure time, three timers (time limit relays) are provided as shown in Fig. 14. The leftmost timer controls the pre-discharge time. According to the duration of discharge, selection between the other two timers, the time ranges of which are limited to 1 min. and 5 min. respectively, can be made by a change-over switch which is a 3-position toggle switch, its central off-position allowing the source to be controlled by hand. Electric signal from this timer circuit can be used as the starting pulse for a device interlocking magnetic shutter and automatic plate racking mechanism of the spectrograph.

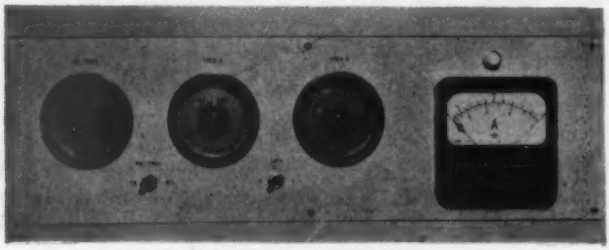

Fig. 14. Timer Panel.

c. Parameter control device

Circuit parameters of every source can be controlled on a panel by switches or devices of several types. They are so arranged that the required control can be made on a sub-panel belonging to the source. If one of the buttons of the selector switch is depressed to select the source, the corresponding sub-panel is illuminated by a pilot lamp, on which sub-panel the required control is made.

At the same time the meters to be used are also indicated by their respective pilot lamps. In spite of the presence of many components to be controlled, confusions are minimized by virtue of the devices described above.

Paractical sequence of control will be briefly described in the following for the case of the spark source as an example. The button of "Raiskij spark" is depressed. The pilot light on the spark sub-panel is lighted. At the same time, compressed air is blown through the control gap by the opening of a magnetic valve, the ultra-violet lamp is illuminated and the enlarged image of the control gap is projected on the screen. Selections of the capacitance and the charging resistance may be made at the same time by a gang switch of small rotary type. Input-voltage may be varied with a momentary type toggle switch which starts a small driving motor to work a slider of auto-transformer. As the switching of high voltage circuit is accomplished by actuation of vacuum switches, change-over of the vacuum switches may be made even when the spark source is running. The voltage at terminals on the panel is D.C. 24 V and not higher.

2. Measure for safety

There are two purposes in installing the safety devices: protection of the operator and protection of various circuit components. For the convenience of inspection of the apparatus, removable doors at the front and rear of the unit, eight in all, are provided. By a guarding device interlocking these doors and the door of the arc-spark stand, removal of any one of the eight doors renders the source inactive. For the safety and the assuarance of reliable action, an independent 6.3 V A.C. network is provided with which the action of control network remains unimpaired when the safety circuit control fails.

This arrangement is very convenient for inspection. A shorting switch for the safety circuit is also provided in the interior of the unit. As a protective device against abnormal operation, over-load circuit breakers are separately and extensively installed in all the circuits. Risk of depending on unreliable fuses is thus eliminated. The over-load breakers are so adjusted that 25% excess of current in normal operation breaks instantly the current. Another precaution taken for the protection of many relay contacts is to let them make or break in no-load condition. For example,

switches, which control capacitance and resistance of the multi-source, are located on a flush panel shown in Fig. 15. A transparent acryl cover is provided on the panel to prevent the operator from touching these control switches. This cover is also included in the interlock guard system. The above measures save the expence of installing heavy-duty relays. In the past two and a half year operation. no serious damages have been caused to the contacts of the relays.

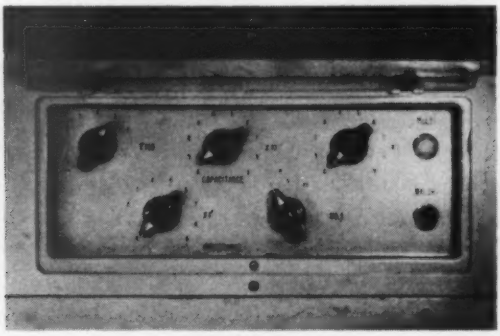

Fig. 15. Flush Panel.

3. Vacuum switch

Vacuum switch is extensively used in high voltage circuits of the unit. A view of the vacuum switch is shown in Fig. 16. This switch was first suggested by the author and Nakano Electronic Industries Co. Ltd., who turned out the present unit,

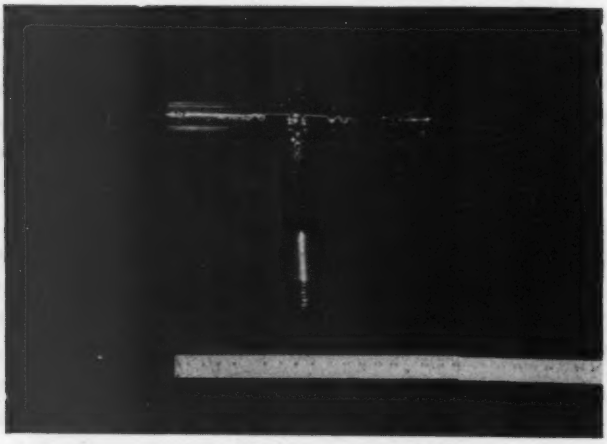

Fig. 16. Vacuum Switch.

undertook its design and production. The performance of the vacuum switch was studied by Jennings et al[16]. The withstand voltage of the vacuum switch is not limited by the internal gap, but by the surface leakage of the glass envelope. One drawback of this switch is the relatively large coil current.

5. Measuring System

What should be measured in the spectrographic light source unit is not precisely known. As already described in the introduction, this ambiguity is from the fact that the correlation between discharge condition and phenomena, such as evaporation and excitation of materials, is not well understood. Many difficulties would still be met even though the purpose of measurement is limited to the supervision on reproducibility of electrical conditions.

Probably, different methods of measurement should be worked out each time when a particular discharge condition is dealt with. See, for example, the literature cited[17)18)]. Such being the case, rough and inaccurate comments on the source condition are seen in the literature of spectrochemical analysis, which makes the comparison between the results obtained at two independent laboratories impossible. Let the author try to illustrate the matter by an example. Fig. 23 shows the voltage wave of a low voltage A.C. arc source. In this case, suitable parameters should be specified for the discharge to be reproducible. Assuming that the line voltage is sinusiodal, the next three quantities should be fixed. They are,

1. Peak values of the voltage wave.
2. Ignition phase (θ) illustrated in Fig. 23.
3. Series impedor of the arc circuit.

It will be excusable to presume —— at least in the author's opinion —— that, for commercially available source units, no regard is being paid to the above, probably because of production cost. Those who are not trained in spectrographical work, when they read the currents as shown in Fig. 23 on a meter calibrated against sinusoidal wave, would report them as the excitation conditions. It will be far better to specify clearly the circuit parameters (C, R and L) than to use customary meters in spectrographic source unit. A typical examples can be seen in New Multi-Source Unit which recently appeared on the market. It has only one meter which reads the input line voltage. Furthermore, for multi-source type discharge, the input voltage is fixed to 230 V and can not be varied. Design, such as the above, seems to be

16) J. E. Jennings, A. G. Schmager and H. G. Ross; Am. Ind. Elec. Eng., **75** (1956) 350.
17) K. Laqua; Spectrochim. Acta, **4** (1952) 446.
18) J. san Calker; Spectrochim. Acta, **5** (1952) 19.

reasonable, especially for the instrument of industrial use when the economical view point is the guiding principle.

But it is not desirable to apply such principle to instruments for research use. After all, it seems practical and convenient to use an oscilloscope and observe the wave form of discharge. But this does not mean that being convenient is being sufficient. As the modern trend of spectrographic source units is in the direction of the so-called "triggered source", the circumstances have become more and more complicated. All of those discharge wave-forms obtained by the "triggered source" are considered to be a train of pulses. Hence, it may be useful to introduce the conceptions and techniques used in pulse technology into practical spectroscopy. However, as too many devices will be required for all-round measurement with as yet no known way of incorporating all of them in one unit, further contemplation on things involved becomes necessary to meet our expectation. Therefore, the measuring scheme is laid according to the following principles.

1. Every source and its detecting elements should be assembled in advance.
2. Detecting elements should be so arranged as to be easily accessible to external measuriug devices.
3. Thermoelectric type meter (RF-meter) should be adopted for measuring the current because the most important parameter for the determination of discharge characteristic of an arc is the arc current.
4. A simple oscilloscope should be used for monitoring the wave forms of discharges; this is not intended for accurate measurement.
5. A phase meter should be provided.
6. A peak voltemeter should be provided.
7. All measuring meters should be of wide-anale type if possible.
8. Digital indication of capacitance and resistance.

Brief explanation of some of the above items which are of some significance will be given in the following.

1. Peak voltmeter

Fig. 17 shows the circuit. M is a wide-angle meter of moving coil type. Peak charging voltage of the capacitor in the cases of multi-source and Walsch source, peak voltage in the case of uni-arc source, and voltage of the continuous D.C. arc are measured with this meter.

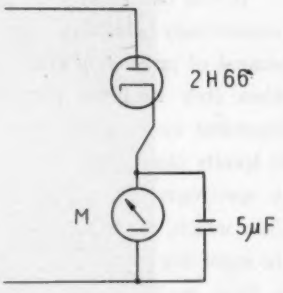

Fig. 17. Peak voltmeter circuit.

2. RF-meter

Two RF-meters are installed. One is used for the measurement of spark current and the other for the average current measurement of triggered sources. The latter is a dual range meter specially designed and made by Yokogawa Electric Works, Ltd.

3. Oscilloscope

Dual trace oscilloscope with 6″ cathode ray tube. The horizontal sweep generator is of Miller's type. An electronic switch is provided to distinguish between two phenomena.

4. C and R indicator

Fig. 18 shows the device used. Five display tubes indicate the capacitance and the resistance inserted in discharge circuits of multi-source and Walsh source. Gang switches control the display tubes automatically.

5. Phase meter

Fig. 18 also shows the iudicator of phase meter. It is calibrated directly against electric degrees and indicates the phase difference between two lines. Principle of the "square wave method" is adopted for the circuit design.

Fig. 18. Display Panel.

6. Layout of the Unit

Fig. 19 shows the overall view of this unit in combination with Jaco 3.4 m plane grating spectrograph. The optical bench of the grating spectrograph is supported by this unit. Shimadzu QF-60 quartz spectrograph is also mounted on the unit. A compact assemblage of electrical appliances as shown in Fig. 19 has generally an advantage of short interconnecting cables being used. In addition, the top of the unit may be used as a working bench. (The top surface is covered with "Decola"

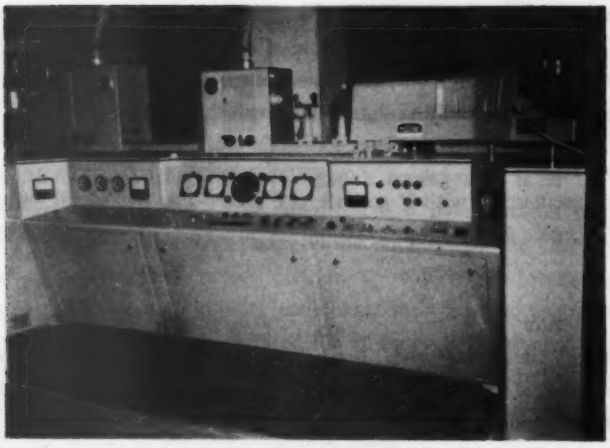

Fig. 19. Over-all view of the unit.

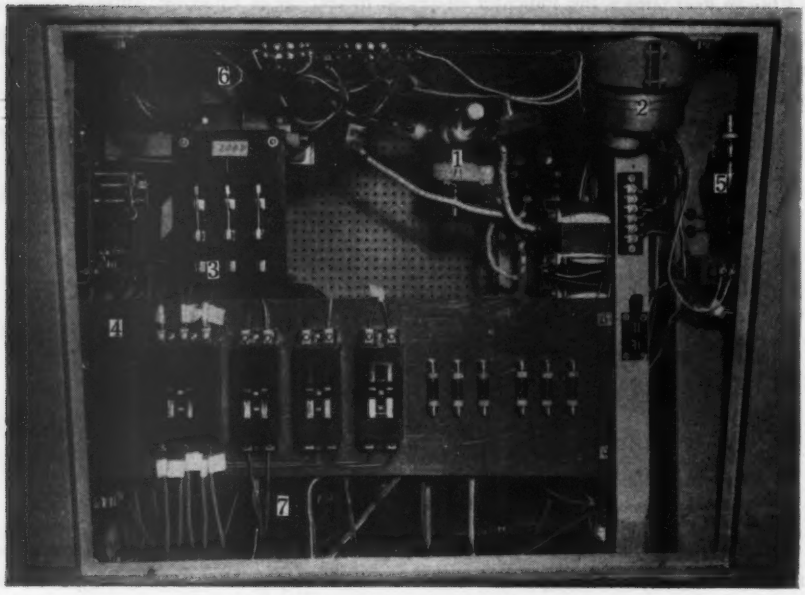

Fig. 20 (a). Interior view of the unit.

1. 6-phase mercury pool rectifier tube.
2. selsin motor.
3. transfer switch, 3-S-1 in Fig. 4.
4. overload breaker board.
5. 2H-66 tube in Fig. 17.
6. driving motor for moving iron core reactor.
7. Δ-YY transformer, 4-T-1 in Fig. 5.

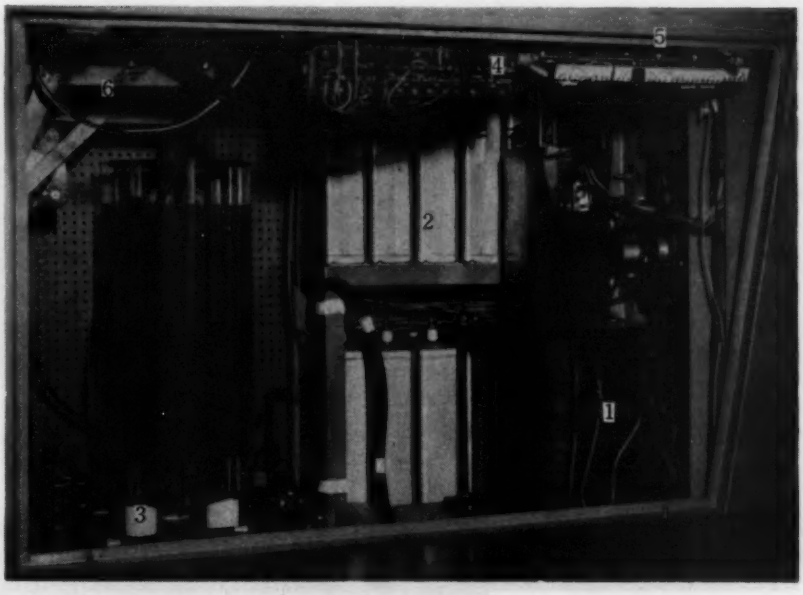

Fig. 20 (b). Interior view of the unit. Electronically controlled igniting pulse generator is removed.

1. moving iron core reactor.
2. capacitor bank.
3. self-inductance, 2-L-2 in Fig. 4.
4. source selector switch.
5. Dekatron-tube counting assembly.
   (part of the electronically controlled igniting pulse generator.)
6. vacuum switch holder.

board for this purpose.) Dimensions of the unit are 340 cm in length, 110 cm in width, and 110 cm in height.

The following rules were observed in assembling the unit. Wiring of high frequency and high voltage parts should be as short as possible with enough spacing between wires. On the other hand, wiring of low frequency and low voltage parts can be long, and wires should be tidied up into as small a space as possible.

To facilitate inspection of the parts, intermediate terminals are provided on many wires.

Fig. 20 shows the interior arrangement of the unit.

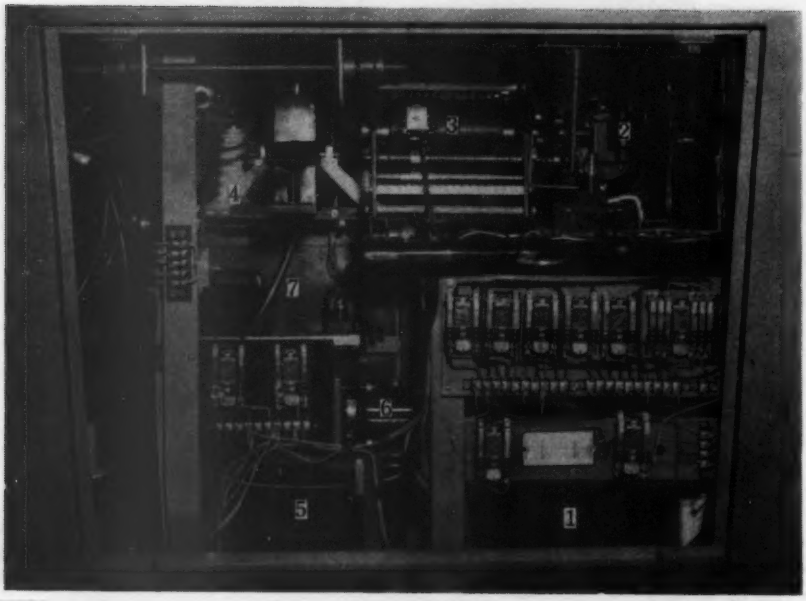

Fig. 20 (c). Interior view of the unit.

1. dry type transformer for high-voltage A.C. arc source, 2-T-1 in Fig. 2.
2. synchronous motor in Fig. 11.
3. cam-shaft interrupter.
4. control gap assembly of the spark source.
5. auto-transformer, 1-T-1 in Fig. 1.
6. driving motor for auto-transformer.
7. power transformer, 1-T-2 in Fig. 1.

7. The Waveforms of Individual Sources

Typical oscillograms of voltage and current obtained by the sources installed in this unit are shown in Fig. 21~Fig. 27.

Acknowledgements

The author wishes to express his thanks to S. Nishiura, director of the Nakano Electronic Ind. Co., Ltd., for undertaking the construction of this unit, and also to H. Kawaguchi, M. Takahashi and K. Takashima for their assistance in preparing this article.

Fig. 21. Illustration of the discharge of spark source. All the oscillograms show the course of voltage in capacitors 1-C-4~7 of Fig. 1.

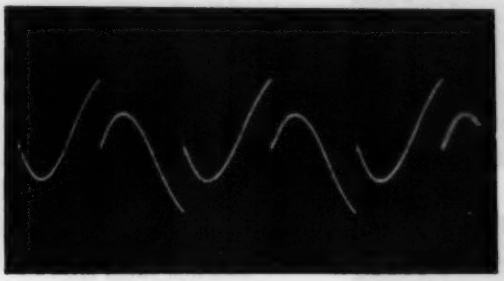

a) One break per half cycle.
C=0.016μF, c. g.=5.0mm
L=250μH, a. g.=2.5mm
R=residual, Input voltage =150V
horizontal sweep rate =5msec/division

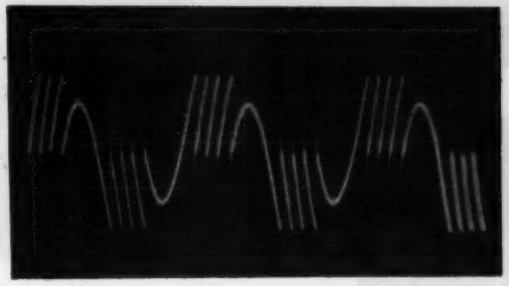

b) Four breaks per half cycle.
C=0.016μF, c. g.=3.0mm
L=250μH, a. g.=2.5mm
R=residual, Input voltage =240V
horizontal sweep rate =5msec/division

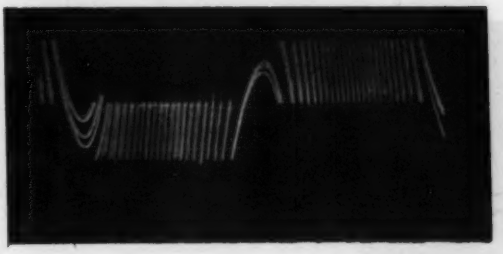

c) 22-breaks per half cycle.
C=0.003μF, c. g.=1.0mm
L=250μH, a. g.=1.0mm
R=residual, Input voltage =240V
horizontal sweep rate =2msec/division

d) Transient oscillating voltage wave.
$C=0.016\mu F$, c. g.=5.0mm
R=residual, a. g.=2.5mm
$L=0\mu H$
horizontal sweep rate
$=10\mu$sec/division

e) Same as d).
$L=250\mu H$
horizontal sweep rate
$=10\mu$sec/division

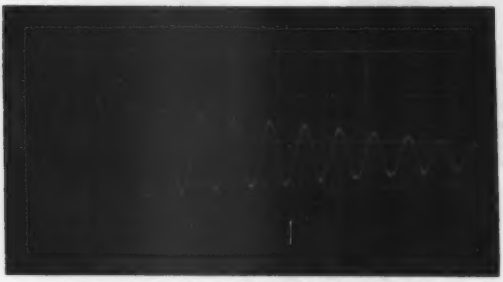

f) Same as d).
$L=1000\mu H$
horizontal sweep rate
$=10\mu$sec/division

g) Same as d).
$C=0.003$, c. g.=6mm
$L=0\mu H$, a. g.=2mm
R=residual
horizontal sweep rate
$=10\mu$sec/division

Fig. 22. Illustration of the discharge of high-voltage A. C. arc source.

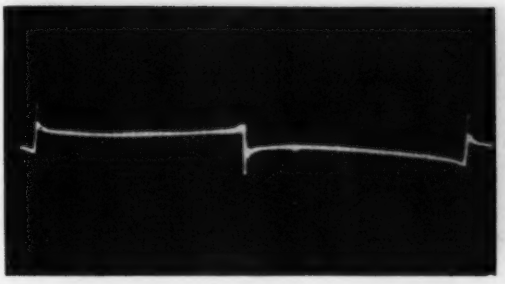

a) Voltage wave.
2400V, 2.3A, a.g.=2.0mm
horizontal sweep rate
=2msec/cm

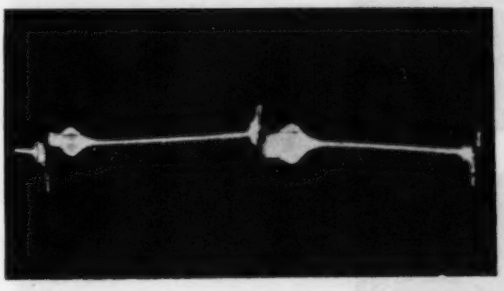

2400V, 2.3A, a.g.<1.0mm
oscillations are observed at
the reignition phase.
horizontal sweep rate
=2msec/cm

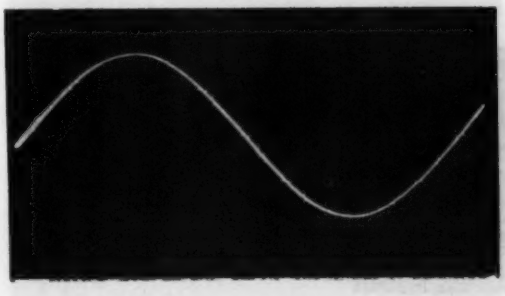

b) Current wave.
2400V, 2.3A, a.g.=2.0mm
horizontal sweep rate
=2msec/cm

Fig. 23. Illustratation of the discharge of low-voltage A. C. arc source.

θ

a) Course of voltage in arc gap. 100c/s ignitions (full wave ignition), θ indicates the phase angle where the igniting pulse occured.

b) Current oscillogram corresponding to a).

c) Course of voltage in arc gap. 50c/s ignitions (half wave ignition).

d) Current oscillogram corresponding to c).

Fig. 24. Illustration of the discharge of interrupted arc source.
All photos are current oscillograms.

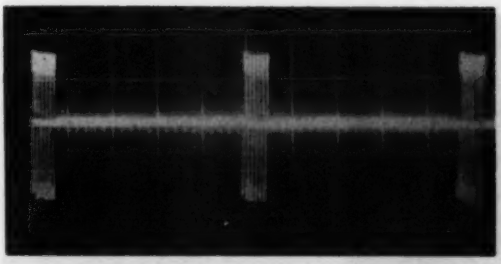

a) Full wave ignition.
Impulse ratio: 6:44

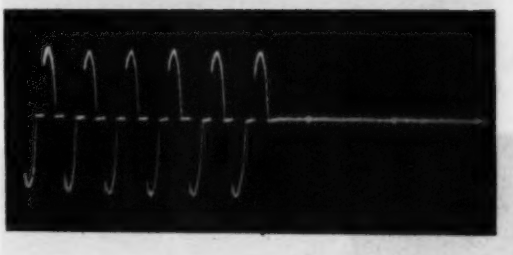

b) Same as a).
horizontal sweep rate is increased.

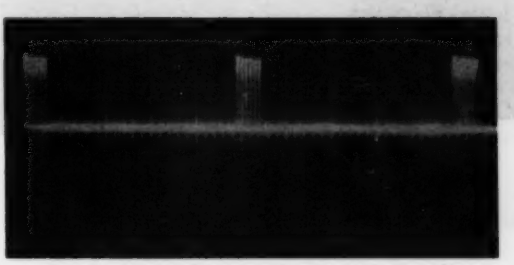

c) Half wave ignition.
Impulse ratio: 6:44

d) Same as c).
horizontal sweep rate is increased.

Fig. 25. Illustration of the discharge of "Uni-arc" source.

a) Voltage oscillogram.
θ represents the ignition phase angle
horizontal sweep rate
=2msec/cm

θ

b) Voltage oscillogram.
horizontal sweep rate
=5msec/cm

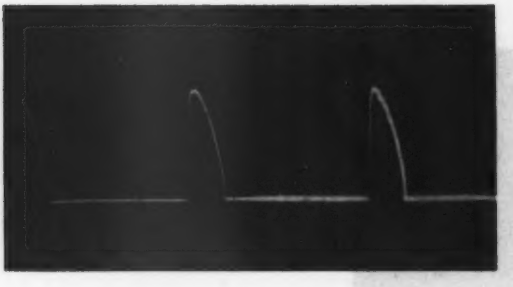

c) Current oscillogram.
horizontal sweep rate
=5msec/cm

Fig. 26. Illustration of the discharge of "Multi-source" type source: Course of the current in capacitor in Fig. 8.

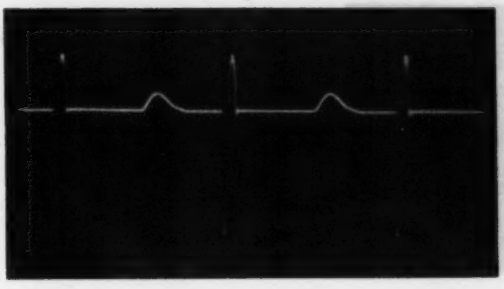

a) oscillogram showing oscillating current.
$C=200\mu F$, $L=800\mu H$,
R=residual
horizontal sweep rate
=5msec/division

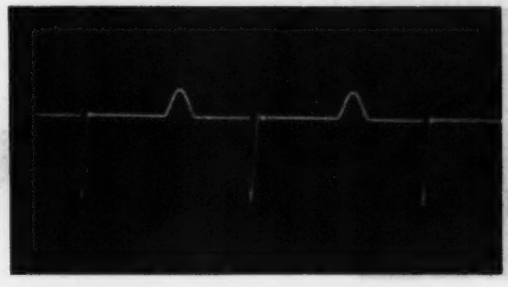

b) oscillogram showing critical damped current.
$C=200\mu F$, $L=800\mu H$,
$R=12\Omega$
horizontal sweep rate
=5msec/division

c) oscillogram showing over-damped current.
$C=200\mu F$, $L=800\mu H$,
$R=30\Omega$
horizontal sweep rate
=5msec/division

Fig. 27. Illustration of the discharge of Walsh source: Course of the current in capacitor 3-C-1~11 in Fig. 8.

a) $C=499\mu$F.
R in charging circuit=20Ω
R in discharge circuit=
residual
$L=800\mu$H
horizontal sweep rate
=5msec/division

b) $C=100\mu$F.
R in charging circuit=40Ω
R in discharge circuit=
residual
$L=800\mu$H
horizontal sweep rate
=5msec/division

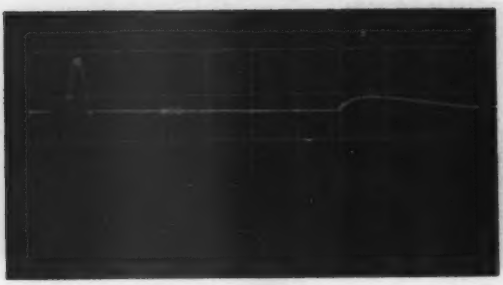

c) $C=30\mu$F.
R in charging circuit=20Ω
R in discharge circuit=
residual
$C=800\mu$H
horizontal sweep rate
=1msec/division